Voltage-dependent Gating of Single Wild-Type and S4 Mutant KAT1 Inward Rectifier Potassium Channels

PAUL C. ZEI*‡ and RICHARD W. ALDRICH*‡

From *The Howard Hughes Medical Institute and ‡Department of Molecular and Cellular Physiology, Stanford University School of Medicine, Stanford, California 94305

ABSTRACT The voltage-dependent gating mechanism of KAT1 inward rectifier potassium channels was studied using single channel current recordings from *Xenopus* oocytes injected with KAT1 mRNA. The inward rectification properties of KAT1 result from an intrinsic gating mechanism in the KAT1 channel protein, not from pore block by an extrinsic cation species. KAT1 channels activate with hyperpolarizing potentials from −110 through −190 mV with a slow voltage-dependent time course. Transitions before first opening are voltage dependent and account for much of the voltage dependence of activation, while transitions after first opening are only slightly voltage dependent. Using burst analysis, transitions near the open state were analyzed in detail. A kinetic model with multiple closed states before first opening, a single open state, a single closed state after first opening, and a closed-state inactivation pathway accurately describes the single channel and macroscopic data. Two mutations neutralizing charged residues in the S4 region (R177Q and R176L) were introduced, and their effects on single channel gating properties were examined. Both mutations resulted in depolarizing shifts in the steady state conductance–voltage relationship, shortened first latencies to opening, decreased probability of terminating bursts, and increased burst durations. These effects on gating were well described by changes in the rate constants in the kinetic model describing KAT1 channel gating. All transitions before the open state were affected by the mutations, while the transitions after the open state were unaffected, implying that the S4 region contributes to the early steps in gating for KAT1 channels.

KEY WORDS: single channel analysis • S4 region • *Arabidopsis thaliana* • site-directed mutagenesis • activation

INTRODUCTION

Potassium channels constitute a functionally and structurally diverse class of ion channels (for reviews see Salkoff et al., 1992; Hoshi and Zagotta, 1993). The majority of voltage-dependent potassium channels can be classified as either outwardly or inwardly rectifying channels that preferentially conduct outward or inward current, respectively. Cloned outward rectifiers, including the delayed rectifier potassium channels, inactivating *Shaker*-family channels (Kamb et al., 1987; Tempel et al., 1987; Pongs et al., 1988), and the Calcium-activated maxi-K channels (Atkinson et al., 1991; Adelman et al., 1992; Butler et al., 1993), share a common putative transmembrane topology consisting of six transmembrane segments, a pore loop between the fifth and sixth transmembrane segments, and an S4 "voltage sensor" region.

Inward rectifier K^+ channels were first described as "anomalous rectification" currents to emphasize the contrast between these channels and previously described outwardly rectifying currents (Katz, 1949; Hille, 1992). Inwardly rectifying currents have been examined in a variety of preparations, including frog skeletal muscle, and tunicate and starfish eggs (Adrian, 1969; Hagiwara and Takahashi, 1974; Hille and Schwarz, 1978). These channels preferentially conduct inward current while limiting outward current. Recently, the cDNA clones and primary amino acid sequences for several inward rectifiers have been obtained. These include the IRK, ROMK, GIRK, K_{ATP}, and KAT1 families (Anderson et al., 1992; Sentenac et al., 1992; Dascal et al., 1993; Ho et al., 1993; Kubo et al., 1993*a,b*; Ashford et al., 1994; Inagaki et al., 1995; Krapivinsky et al., 1995). Unlike the proposed transmembrane topology of outwardly rectifying potassium channels, the "small" inward rectifiers possess two putative transmembrane regions, with a pore region interposed between them. The NH_2 and COOH termini of these channels are relatively long and intracellularly located. This proposed structure has been recently confirmed using x-ray crystallography in the bacterial potassium channel KcsA (Doyle et al., 1998). In the cloned small inward rectifiers, intracellular Mg^{2+} and polyamines (spermine, spermidine, and putrescine) have been demonstrated to be the intracellular blocking particles responsible for inward rectification (Kubo et al., 1993*a,b*; Ficker et al., 1994; Lopatin et al., 1994; Nichols et al., 1994; Fakler et al., 1995).

Dr. Zei's current address is Dept. of Internal Medicine, Brigham and Women's Hospital, 75 Francis Street, Boston, MA 02115.

Address correspondence to Richard W. Aldrich, Dept. of Molecular and Cellular Physiology, Beckman Center B171, Stanford, CA 94305-5426. Fax: 650-725-4463; E-mail: raldrich@leland.stanford.edu

Among inwardly rectifying potassium channels, the KAT1 and akt1 channels are unique in both structure and function. KAT1 and the related channel akt1 are inwardly rectifying potassium channels cloned from the plant *Arabidopsis thaliana*, a member of the mustard family, through a yeast complementation strategy (Anderson et al., 1992). Unlike the small inward rectifiers, KAT1 possesses six putative transmembrane regions, a pore loop between the fifth and sixth transmembrane regions, and an S4 motif. Structurally, KAT1 resembles the *Shaker* family of potassium channels, and yet functionally it behaves as an inward rectifier (Schachtman et al., 1992). Unlike the small inward rectifiers, KAT1 rectification does not require intracellular cation block (Hoshi, 1995). Inward rectification is not significantly altered upon patch excision, suggesting that polyamine block is also not important in KAT1 rectification (Hoshi, 1995). It is therefore a reasonable conclusion that the gating mechanisms resulting in an inwardly rectifying phenotype in KAT1 are intrinsic to the channel protein itself.

KAT1 appears to have the structural architecture of an outward rectifying channel, yet its functional phenotype is that of an inward rectifier. This suggests that perhaps KAT1 achieves inward rectification through a fast inactivation recovery mechanism, as demonstrated in the *eag*-family channel herg (Smith et al., 1996; Spector et al., 1996) and in *Shaker* channels containing mutations that alter activation properties (Miller and Aldrich, 1996). However, NH_2-terminal deletions and permeant ion effects that should affect NH_2-terminal inactivation processes (Demo and Yellen, 1991; Lopez-Barneo et al., 1992) and mutations in residues corresponding to residues critical for C-type inactivation (Hoshi et al., 1991; Heginbotham and MacKinnon, 1992) in *Shaker* channels have little effect on KAT1 activation (Marten and Hoshi, 1997). Perhaps the KAT1 protein functions similarly to outwardly rectifying channels like *Shaker,* but is inserted in the membrane in a reversed topology so that the "voltage sensor" is oriented in the electric field in the opposite direction from these other channels. This hypothesis is unlikely, as sequence analysis does not suggest possible signal sequences in the channel protein that differ significantly from those of other channels, and mutations in the NH_2 terminus do not reverse the channel's voltage dependence, as might be expected if there were a crucial signal sequence (Marten and Hoshi, 1997). One can also imagine a channel in which states that are normally closed are conducting states, and vice-versa, resulting in opening at negative voltages. In other words, KAT1 may possess a unique gating mechanism in which the polarity of a critical component of the voltage sensing mechanism is reversed so that hyperpolarization, rather than depolarization, increases open probability. Mutations in both the NH_2- and COOH-terminal domains produce significant effects on the voltage-dependent gating behavior of KAT1, suggesting that these regions of the molecule play an important role in gating (Marten and Hoshi, 1997). On the other hand, the presence of the charged S4 voltage sensor motif implies that KAT1 gating involves the S4 region, as seen in other channels gated by voltage.

In other voltage-dependent ion channels, the role of the S4 region in gating has been substantiated through mutagenesis. Mutations of the charged residues located within the S4 segment have been shown to alter the voltage-dependent gating properties of potassium and sodium channels (Stühmer et al., 1989; Papazian et al., 1991; Logothetis et al., 1992, 1993; Schoppa et al., 1992; Tytgat and Hess, 1992; Aggarwal and MacKinnon, 1994). Cysteine mutagenesis has demonstrated that the S4 region likely moves during the activation of sodium channels (Yang and Horn, 1995) and potassium channels (Larsson et al., 1996). Optical signals from channels with fluorescent labels in the S4 region support the hypothesis that the S4 region moves during activation (Mannuzzu et al., 1996; Cha and Bezanilla, 1997). However, mutations in other regions of the channel protein (Gautam and Tanouye, 1990; Lichtinghagen et al., 1990; MacKinnon, 1991; Schoppa et al., 1992; Papazian et al., 1995) have also been shown to alter the voltage-dependent properties of these channels, demonstrating that other channel regions are also likely to be involved in the gating process. Moreover, the S6 region is believed to be involved in the gate that physically impedes ion flux through the channel pore (Liu et al., 1997).

In this article, the gating properties of the wild-type KAT1 channel will be described through the analysis of single channel patch clamp currents. Statistical analysis of the single channel open and closed durations will provide information about conformational changes that the channel undergoes between closed and open states. Analysis of these data can be used to create a kinetic model that accurately describes the gating behavior of the KAT1 channel, particularly conformational transitions near the open state, over a wide voltage range. This kinetic model can then provide insight into the intrinsic voltage-dependent gating properties of KAT1 that result in inward rectification. This model will serve as a basis for interpreting the effects of two neutralization mutations in the S4 region (R177Q and R176L) on the gating mechanisms of KAT1 that produce inward rectification.

METHODS

Molecular Biology

All currents were recorded from the KAT1 channel cloned from the plant *A. thaliana*, which was provided to us by Dr. Richard

Gaber (Northwestern University, Evanston, IL). All mutant constructs were made in the wild-type KAT1 clone using the standard PCR-based cassette mutagenesis. DNA sequences for all mutants were confirmed by dideoxy termination sequencing (Sanger et al., 1977). The KAT1 and mutant cDNA clones were propagated in the λ-YES vector provided by Dr. Gaber in the *Escherichia Coli* strain DH5-α. The cDNA was transcribed in vitro into cRNA using a T7 polymerase (Ambion Inc., Austin, TX). Approximately 40 nl of cRNA per cell was injected into *Xenopus* oocytes to record macroscopic currents. Single channel patches were obtained by injecting cRNA that was diluted up to 1,000-fold. Recordings were made 2–7 d after cRNA injection.

Electrophysiology

Data from single channel patches were recorded in the inside-out configuration, unless otherwise noted (Hamill et al., 1981). Patch pipettes were composed of borosilicate glass (VWR Micropipettes, West Chester, PA). Their tips were coated with wax (Sticky Wax, Emeryville, CA) and fire polished before use. Data were acquired using an Axopatch 200-A patch clamp amplifier (Axon Instruments, Foster City, CA), and the amplifier output was low-pass filtered through an eight-pole Bessel filter (Frequency Devices, Inc., Haverhill, MA), digitized at a frequency as noted in the figure legends and stored for later analysis. The data were typically filtered at frequencies ranging from 400 to 1,000 Hz, which did not limit the kinetic measurements, as KAT1 channel kinetics are relatively slow. A Digital Equipment Corp. LSI 11/73–based minicomputer system (Indec Systems, Sunnyvale, CA) was used for controlling the voltage-clamp protocols and was used for a portion of the data analysis. Experiments were carried out at 20–22°C. The pipette potential was nulled just before seal formation. The voltage error due to junction potentials was estimated to be <5 mV, and no corrections were made for this error. Unless otherwise noted, the holding potential was −40 mV for wild-type KAT1 currents and 0 mV for R177Q and R176L mutant currents.

Data were recorded and stored on the LSI 11/73-based minicomputer system. Voltage pulses were applied every 2–5 s. Linear leak currents and uncompensated capacity currents were subtracted using leak templates made from fits to sweeps with no openings. For the ensemble averages and duration histograms, opening and closing transitions were detected using a 50% amplitude criterion of the single channel amplitude at any given voltage. Open and closed durations were measured from these idealized records. The number of channels in any given patch was determined by observing the maximum number of channel openings at a potential where the probability of the channel being open was high. Unless otherwise noted, single channel patches were used in the data presented in this article.

A confounding factor in the measurement of single channel KAT1 currents is that channels will occasionally exhibit rundown, or a progressive decline in macroscopic current amplitude and open probability over time. It has been noted that rundown is faster in excised patches (Hoshi, 1995). Rundown was indeed occasionally observed in our single channel patches, and the data from those patches were not used.

Duration Fitting and Simulations

Durations of open and closed events were compiled from the idealized single channel data and transferred to a Macintosh-based computer system. Ensemble averages that have been expressed as open probabilities were determined by dividing the current averages by the number of channels in the patch and the unitary current amplitude. The open and closed durations were fitted with sums of exponential probability density functions using the maximum likelihood method. The fits were corrected for the left censor time, or the dead time of the recording system, and for the right censor time, which corresponds to the limited pulse duration (Colquhoun and Hawkes, 1982; Lawless, 1982; Hoshi and Aldrich, 1988). The left censor time was estimated as $0.253/f$, where f represents the filter cutoff frequency in Hertz. The first latency distributions were corrected for the filter delay time, which was estimated as $0.506/f$. Unless otherwise noted, open- and closed-duration histograms are displayed using a log-binning transformation (Sigworth and Sine, 1987) to optimize the presentation of data and associated fits.

Correction for Missed Events

Rate constant values in the three-state burst model described in this article were estimated with corrections for events too short to be resolved (Blatz and Magleby, 1986). Given the model considered and the dead time of the recording system, the four effective rate constants were calculated by estimating the fraction of all events in each data set both longer and shorter than the dead time of the recording system. The rate constant values were then optimized separately for the open and closed-time parameters.

Solutions

All currents were recorded in symmetrical 140-mM K^+ solutions. The standard extracellular solution contained (mM): 140 KCl, 6 $MgCl_2$, 5 HEPES, pH 7.2. The intracellular solution contained (mM): 140 KCl, 11 EGTA, 2 $MgCl_2$, 1 $CaCl_2$, 10 HEPES, pH 7.2.

RESULTS

Single Channel Currents

Although macroscopic patch data can provide a great deal of insight into the gating behavior of KAT1 channels, single channel analysis allows the observation of real-time conformational changes of individual KAT1 protein molecules that can constrain a potential kinetic model. Fig. 1 *A* displays representative KAT1 single channel currents over a voltage range from −110 through −190 mV. After pulse initiation, there is a short delay before the channel initially opens. This delay, or first latency to opening, becomes faster with increasingly negative voltages. Once open, the channel flickers, or bursts, between open and closed states before occasionally entering a longer-lived closed state. From this longer-lived closed state, the channel may begin bursting again. With increasingly negative voltages, KAT1 channels are more likely to continue bursting through the entire pulse duration. The combined effect of shorter latencies to first opening and longer burst durations is an increasing overall open probability with increasing hyperpolarization.

A current–voltage relationship [i(V)][1] constructed from single channel currents yields a unitary conductance of ∼7.5 pS in symmetrical 140-mM K^+ solutions

[1]*Abbreviations used in this paper:* G(V), conductance–voltage; i(V), current–voltage relationship.

(Fig. 1 *B*). The i(V) relationship is linear over the range of activating voltages examined for KAT1 single channels, confirming that, in this voltage range, gating mechanisms, not permeation properties, determine inward rectification. At depolarized potentials (greater than +20 mV), outward current is not observed in KAT1 channels (data not shown), which is in agreement with the observation of open-channel rectification of outward currents in macroscopic tail currents (Zei, 1998). KAT1 currents at voltages more hyperpolarized than −200 mV were difficult to obtain, a result of both the extreme voltages and the long pulse durations needed.

The overall behavior of single KAT1 channels at a given potential is demonstrated by the ensemble averages expressed as open probabilities in Fig. 2 *A* over a range of voltages. The overall time course of activation is very similar to currents recorded in macroscopic patches (Hoshi, 1995; Zei, 1998), in the whole-cell voltage clamp configuration (Schachtman et al., 1992; Véry et al., 1995; Marten and Hoshi, 1997), and in the cut-open oocyte system (our unpublished results), confirming that the single channel records accurately represent the gating behavior of wild-type KAT1. The channels activate slowly after a small but noticeable delay, with a time scale on the order of several hundred milliseconds, in contrast with activation in *Shaker* channels, which occurs on the order of 1–10 ms. This delay suggests the existence of multiple closed states along the activation pathway. The time course of activation becomes faster with increasingly negative voltages ranging from −110 to −190 mV, and there is no appreciable decay or inactivation in the ensemble average currents. The steady state probability that the KAT1 channel is open during the pulse increases with increasingly negative voltages, as shown in Fig. 2 *B*. The open probability increases steeply between −120 and −180 mV, saturating between −190 and −200 mV. The maximum open probability is ~0.7, reflecting a significant contribution of closed events to the steady state channel behavior even at the most hyperpolarized potentials. The open probability voltage dependence is fitted by a Boltzmann function:

$$P_o = P_o^{max}\left[\frac{1}{1 + e^{-(V - V_{1/2})zF/RT}}\right], \quad (1)$$

represented by the solid line in Fig. 2 *B*, where P_o is open probability, P_o^{max} is maximal open probability observed, $V_{1/2}$ is the voltage at which the open probability is 0.5 of P_o^{max}, z is the apparent gating valence, and F, R, and T have their usual meanings. The midpoint of activation ($V_{1/2}$) is extremely negative, estimated at −143 mV, and the apparent charge is relatively small, at −1.4 *e*. In Fig. 2 *B*, the Boltzmann fit obtained from the macroscopic conductance–voltage [G(V)] data (Zei, 1998) is

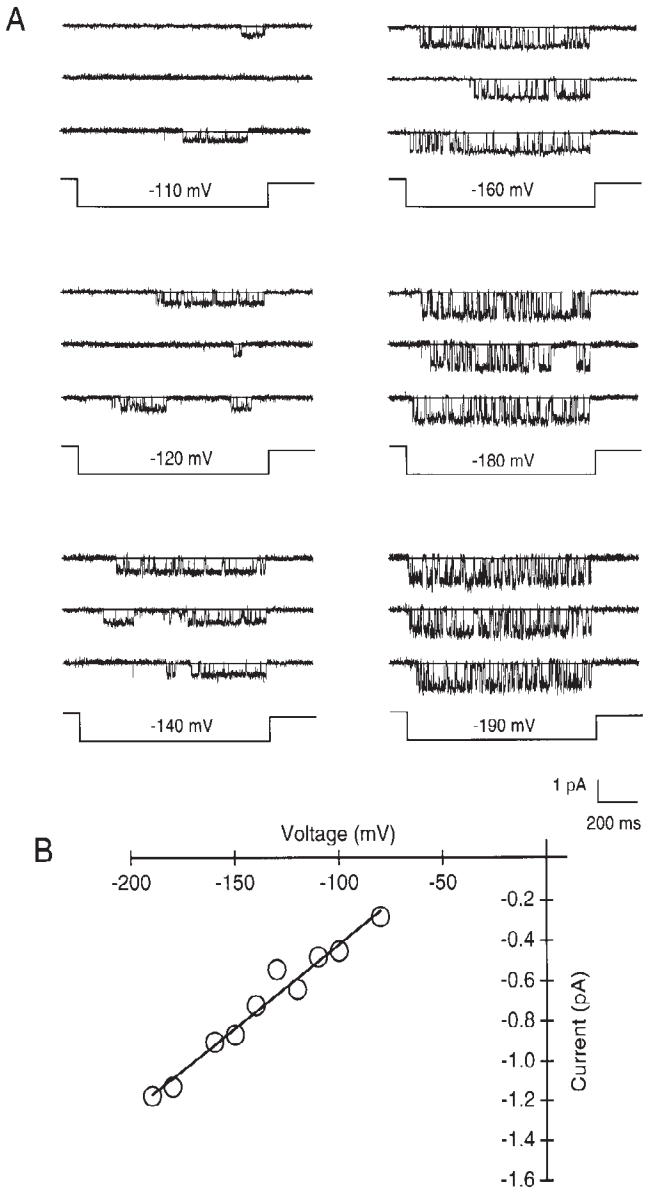

FIGURE 1. (*A*) Representative single channel currents from KAT1 channels recorded in the inside-out patch configuration in response to hyperpolarizing voltage pulses. The voltages are indicated in the figure. The data at −190, −180, −160, −140, −120, and −110 mV were filtered at 0.9, 0.6, 0.6, 0.6, 0.6, and 0.7 kHz, respectively, and sampled at 1.54 kHz. The voltage pulses were delivered every 2–6 s. The prepulse, tail, and holding potentials were −40 mV. (*B*) The single open channel i(V) for KAT1 channels over the voltage range from −80 mV to −190 mV. Current amplitudes were obtained as follows: at each given voltage, all sampled data points from a representative sweep were compiled into histograms plotting the number of data points as a function of current amplitude. These current amplitude histograms were then fitted by eye to determine peak amplitudes, which represent closed and open state current values. The single channel current amplitude was then calculated as the difference between the open and closed state current levels at each given potential. The i(V) curve has been fitted to a linear function, which yields a unitary conductance of 7.5 pS.

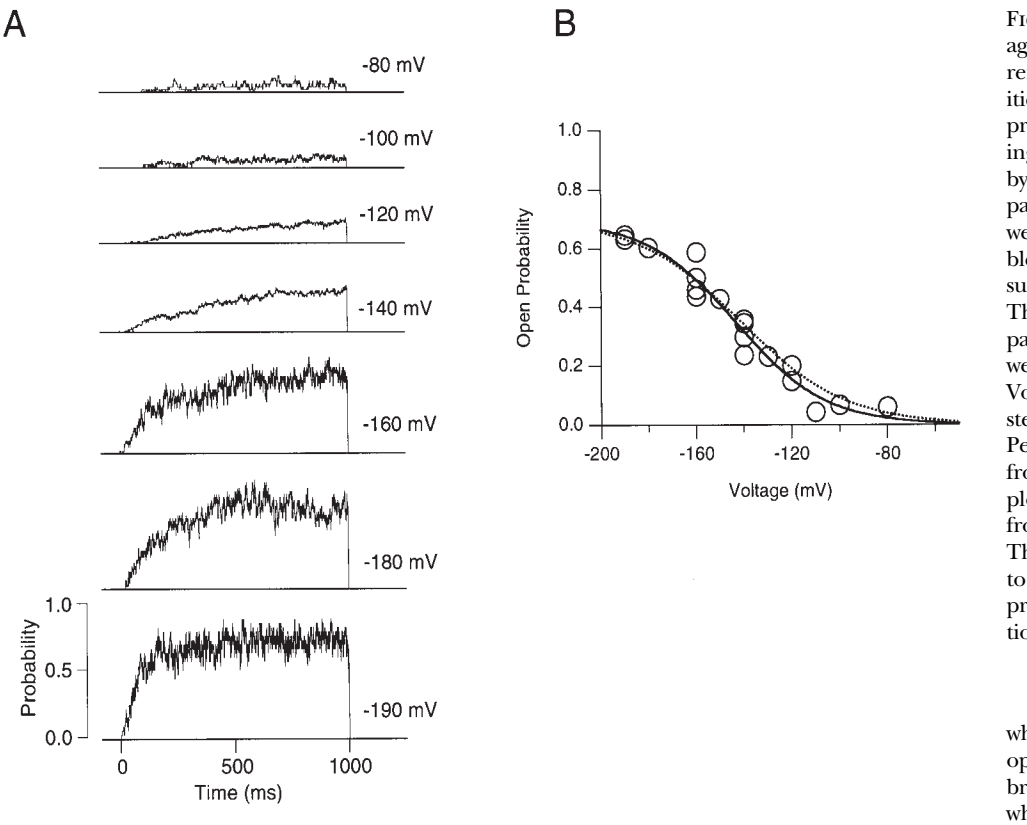

FIGURE 2. (*A*) Ensemble averages of single-channel patch currents expressed as open probabilities at several voltages. Open probability is calculated by dividing the ensemble average current by the number of channels in the patch (single channel patches were used in most of the ensemble averages shown) and the measured unitary current amplitude. The voltages are indicated in the panel. Recording conditions were as described in Fig. 1. (*B*) Voltage dependence of the steady state open probability. Peak probabilities recorded from the ensemble averages are plotted against voltage. Data from several patches are shown. The smooth curve represents a fit to a Boltzmann function expressed by the following equation:

$$P_o = P_o^{max}\left[\frac{1}{1 + e^{-(V - V_{1/2})zF/RT}}\right],$$

where P_o^{max} is the maximum open probability (0.7), V is membrane voltage, $V_{1/2}$ is the voltage where the Boltzmann distribution is equal to 0.5 (−143 mV), z is the equivalent charge movement associated with the Boltzmann distribution (1.36 electronic charges), F is Faraday's constant, R is the universal gas constant, and T is the absolute temperature. The dotted line represents the Boltzmann fit to the macroscopic G(V) relationship (Zei, 1998). The macroscopic G(V) fit has been scaled to the maximum single channel open probability, P_o^{max}.

superimposed and scaled to the maximum open probability derived from the Boltzmann fit to the ensemble average G(V). This comparison demonstrates good agreement between the steady state activation properties observed in both macroscopic and single channel patches.

The voltage dependence of KAT1 activation derived from macroscopic currents is far weaker than that seen in other voltage-gated ion channels. For instance, the apparent gating valence of the *Shaker* channel as measured by limiting slope, Boltzmann fits to tail currents, gating current, and toxin labeling measurements all yield a gating valence of ~12–16 elementary charges per channel (Schoppa et al., 1992; Aggarwal and MacKinnon, 1994; Zagotta et al., 1994*a*). The apparent gating valence of the Ca^{2+}-activated K^+ channel (slo, BK, or maxi-K channel) using limiting slope and Boltzmann fit techniques is between 1.1 and 1.8 *e* (Cox et al., 1997; Cui et al., 1997). However, the slo channel is gated by both voltage and calcium ions.

Transitions Before First Opening

As shown in the representative single channel currents in Fig. 1 *A*, the time to first opening, or first latency, becomes shorter with increasingly negative potentials. During these first latencies, the channel is presumed to traverse closed states along the activation pathway. In Fig. 3 *A* (*top*), cumulative distributions of latencies to first opening are displayed for voltages from −110 through −190 mV. Fig. 3 *A* (*bottom*) depicts the same cumulative first latency distributions scaled to the same steady state probability to facilitate comparison of their time courses. Similar to the activation of macroscopic ionic currents, there is only a small amount of sigmoidicity in the first latency time courses across all voltages examined, indicating only a few discernible closed states in the transitions before first opening. The first latency time course becomes faster with increasingly negative potentials, consistent with the voltage dependence of the macroscopic activation time course.

The voltage dependence of first latencies can be quantified by plotting the median first latency as a function of voltage, as in Fig. 3 *B*. The median first latency is highly voltage dependent, which implies that much of the voltage dependence of activation can be accounted for by the transitions before first opening. Furthermore, if the transition rate constants leaving the open state do not significantly contribute to the ac-

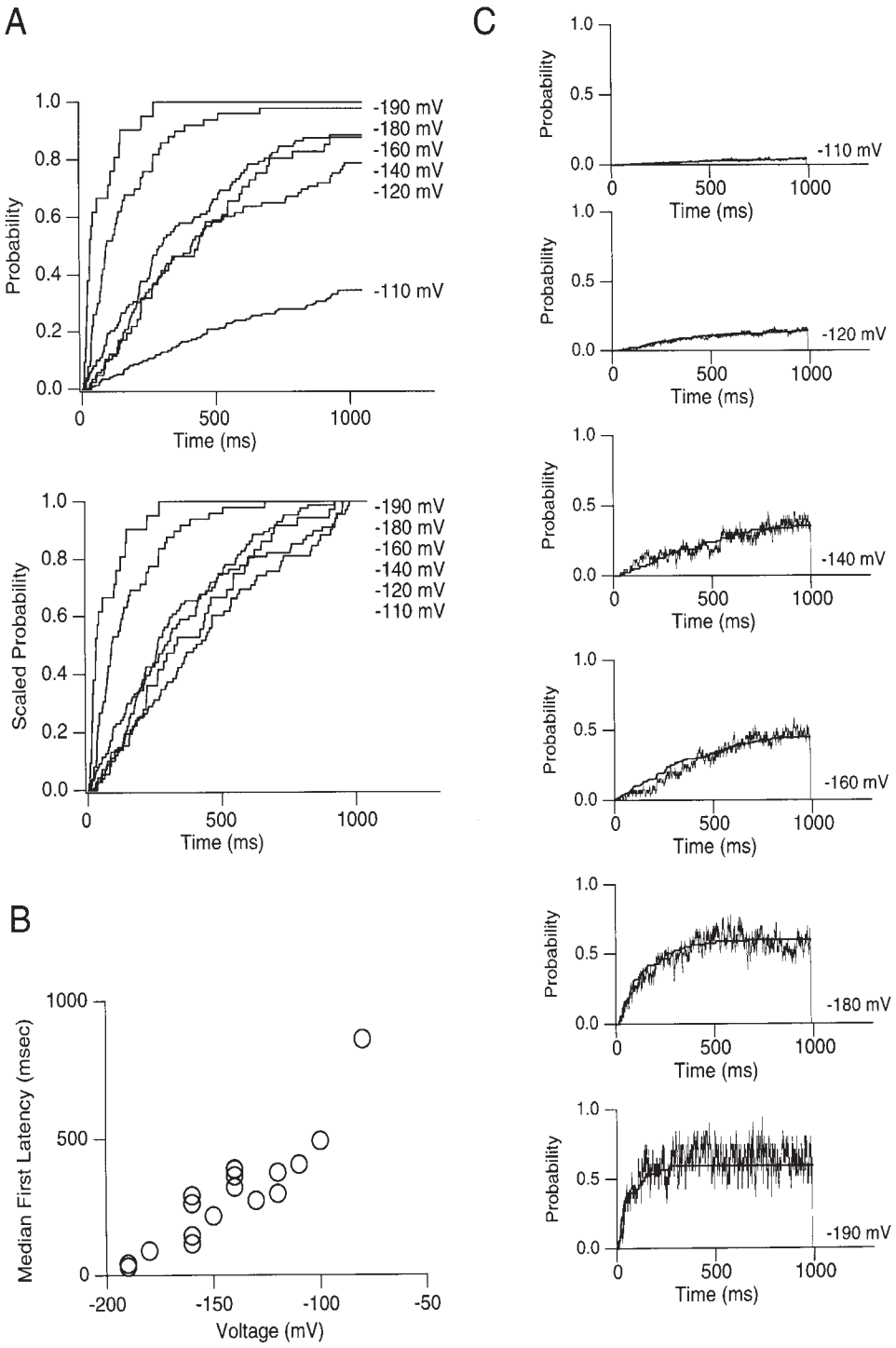

FIGURE 3. (*A*) Cumulative distributions of first latencies recorded at several voltages. The distributions show the probabilities that the channel first opened by the times indicated. The openings were elicited in response to 1,000-ms pulses from a prepulse potential of −40 mV. (*Bottom*) The cumulative first latency distributions have been scaled to a probability of 1 to compare their time courses. (*B*) Median first latencies measured from the distributions in *A* and several additional patches are plotted as a function of pulse potential. Several different patches are represented among the data points. (*C*) The cumulative first latency distributions are superimposed on the ensemble averages from the same patch at each voltage indicated. The thin, relatively noisy lines represent the ensemble averages, and the thick, smoother lines represent the first latency distributions. The curves are scaled so that the steady state levels coincide.

tivation kinetics of KAT1, then the time courses of first latencies and overall activation will be similar. Superimposed cumulative first latency distributions and ensemble averages are shown in Fig. 3 *C* at several voltages. The first latency distributions are normalized to the ensemble averages to facilitate comparison of their time courses. The observed similarity between the first latency and ensemble average time courses over the entire voltage range of activation indicates that indeed much of the voltage dependence of activation results from transitions before the channel first opens.

As seen in Fig. 3 *A*, the first latency distributions saturate at a probability of one only at the most negative voltages, reflecting the fact that, at most voltages, there are several sweeps during which the KAT1 channel fails to open. In fact, the fraction of sweeps that fail to

elicit at least one channel opening is larger at more positive potentials and decreases with increasingly negative voltages. There are several mechanistic possibilities, individually or in combination, that can account for these blank sweeps. First, the channel may enter an inactivated state from a closed state located along the activation pathway. Second, the channel may occasionally enter an inactivated state located after the open state and outside the activation pathway during the previous pulse, from which it does not recover. Third, the first latencies may occasionally be longer than the pulse durations used, particularly at depolarized voltages.

In the first two possibilities, an inactivated state with a relatively slow rate of recovery and, therefore, a long dwell time would result in blank sweeps that tend to cluster together. The tendency for blank sweeps to cluster can be tested with runs analysis (Horn et al., 1984). In runs analysis, a run is defined as a contiguous series of like events. In a system with two types of events, the probability of having R runs in an experiment can be calculated. Given a data set with at least ~40 events, the distribution of R can be approximated by an asymptotic distribution, from which a standard variable, Z, can be defined with a mean of zero and variance of one (Horn et al., 1984):

$$Z = -\frac{R - 2nP(1-P)}{2n^{1/2}P(1-P)}, \qquad (2)$$

where R is the number of runs in the experiment, n is the total number of events, and P is the probability of observing a sweep with at least one opening. Negative Z values indicate a tendency for sweeps to alternate between one or the other type of event, while positive Z values indicate the tendency for like events to cluster in long runs. A Z value greater than +1.6 indicates statistically significant clustering (Horn et al., 1984). Fig. 4 *A* plots the number of openings per sweep contiguously for two experiments at −110 and −140 mV. It might seem qualitatively apparent that there are several clusters of blank sweeps in these experiments. However, in Fig. 4 *B*, the Z values at all voltages with a significant number of blank sweeps do not demonstrate statistically significant clustering, implying that a long-lived inactivated state is unlikely to account for the observation of blank sweeps in KAT1. Furthermore, variation of the interpulse interval between 1 and 6 s did not have a significant effect on the observed frequency of

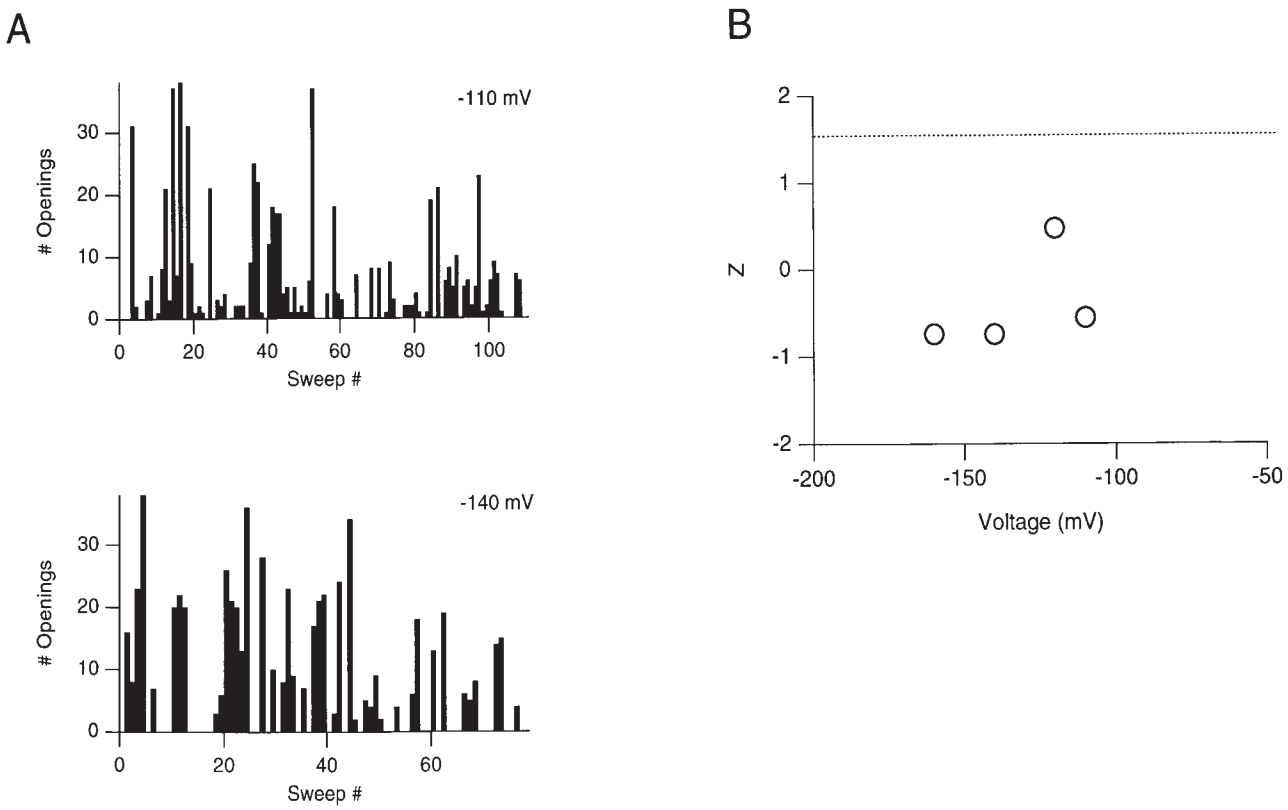

FIGURE 4. (*A*) The number of openings per sweep over an entire experiment are plotted contiguously at −110 and −140 mV. The x-axis indicates consecutive sweep number. The data represent two different patches. (*B*) The test parameter (Z) for runs analysis (see text) is plotted at several voltages. Only those experiments with a significant number of blank sweeps are shown. The dotted line represents a Z value of 1.6. Z values greater than or equal to 1.6 indicate statistically significant clustering of blank sweeps.

blank sweeps (data not shown). These observations suggest that, if the channel enters an inactivated state either along the activation pathway or after the open state, then the recovery rate from that state is fast enough so that the probability of observing blank sweeps is not significantly affected by the interpulse duration, and clustering of blank sweeps is not observed. The possibility that first latencies longer than the pulse duration contribute to the observation of blank sweeps must also be considered. The potential contribution of these various mechanisms to the occurrence of blank sweeps will be discussed further when specific models of KAT1 gating are considered.

Transitions After First Opening: Open States

Opening and closing events were assumed to behave as time-homogeneous Markov processes, so the distribution of open and closed durations can therefore be fitted with a sum of exponential functions. The number of exponential functions that best fits each distribution indicates the minimum number of discernible states at each particular current amplitude. Fig. 5 *A* shows the distributions of open durations at voltages between −110 and −190 mV fitted with single exponential functions. Fits to sums of greater than one exponential did not yield significantly improved fits to the open time distributions using the maximum likelihood method. A good fit of the open time distribution with a single exponential function indicates that there is only one discernible open state. The time constants derived from fits to open time distributions are plotted as a function of voltage in Fig. 5 *B*. Open times become shorter with increasing hyperpolarization, even after the data are corrected for missed events. Since the overall rate of leaving the open state becomes faster with increasing hyperpolarization, at least one of the individual leaving rates should reside outside the activation pathway towards first opening. Otherwise, if all transitions away from the open state were to lie within the activation pathway, as shown below (Scheme I), then the voltage dependence of the sole transition rate constant leaving the open state would be in the opposite direction to that of overall activation, which is mechanistically unlikely, although certainly possible. On the other hand, if at least one of the closed states lies outside of the activation pathway (Scheme II), then the transition from the open to the closed state outside the activation pathway (*rightward arrow*) can become faster with hyperpolarization, which is congruent with the overall voltage dependence of activation, and yet still accounts for the voltage dependence of the mean open times. More complex models that incorporate opposite voltage dependences of individual rate constants and overall activation are certainly physically possible. However, the simpler scheme (Scheme I) was adequate to explain the features of gating (see below). A voltage-dependent open time distribution differs from results seen in *Shaker* channels, where the transitions between the open and closed states outside the activation pathway (C_f and C_i) are essentially voltage independent (Hoshi et al., 1994).

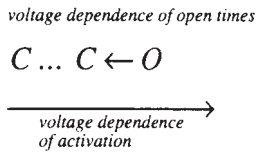

(SCHEME I)

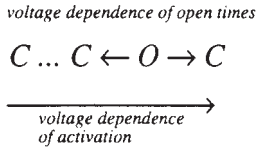

(SCHEME II)

Transitions After First Opening: Closed States

The distribution of closed times that occur after the channel first opens is shown in Fig. 6 *A* at voltages ranging from −110 to −190 mV. The data are well fit by a sum of two exponential functions using the maximum likelihood method, and greater than two exponentials did not significantly improve the fits. This implies that there are at least two discernible closed states in close topological proximity to the open state. As seen in the representative traces in Fig. 1 *A*, the two kinetically distinct closed states can be qualitatively discerned as long and brief populations of closed durations. This type of behavior can be described as bursting behavior, as the channel flickers rapidly between closed and open states in "bursts," with occasional sojourns into a longer-lived closed state, an interburst interval. In Fig. 6 *B*, the long and brief component time constants from the two-exponential fits to closed-time distributions are plotted separately as functions of voltage. The long time constant becomes shorter with more negative voltages, while the brief component is essentially voltage independent. The relative amplitudes of the long and brief components are also shown as functions of voltage (Fig. 6 *B*). Over the entire voltage range examined, the contribution of brief closed events is much greater than that of long closed events.

The gating behavior of KAT1 single channel currents can be analyzed in greater detail using burst analysis (Colquhoun and Hawkes, 1995). As shown in the representative traces of Fig. 1 *A*, bursts appear to become longer, the number of bursts per sweep appears to increase, and the time between each burst appears to decrease with increasing hyperpolarization. These qualitative observations will be confirmed by quantitative

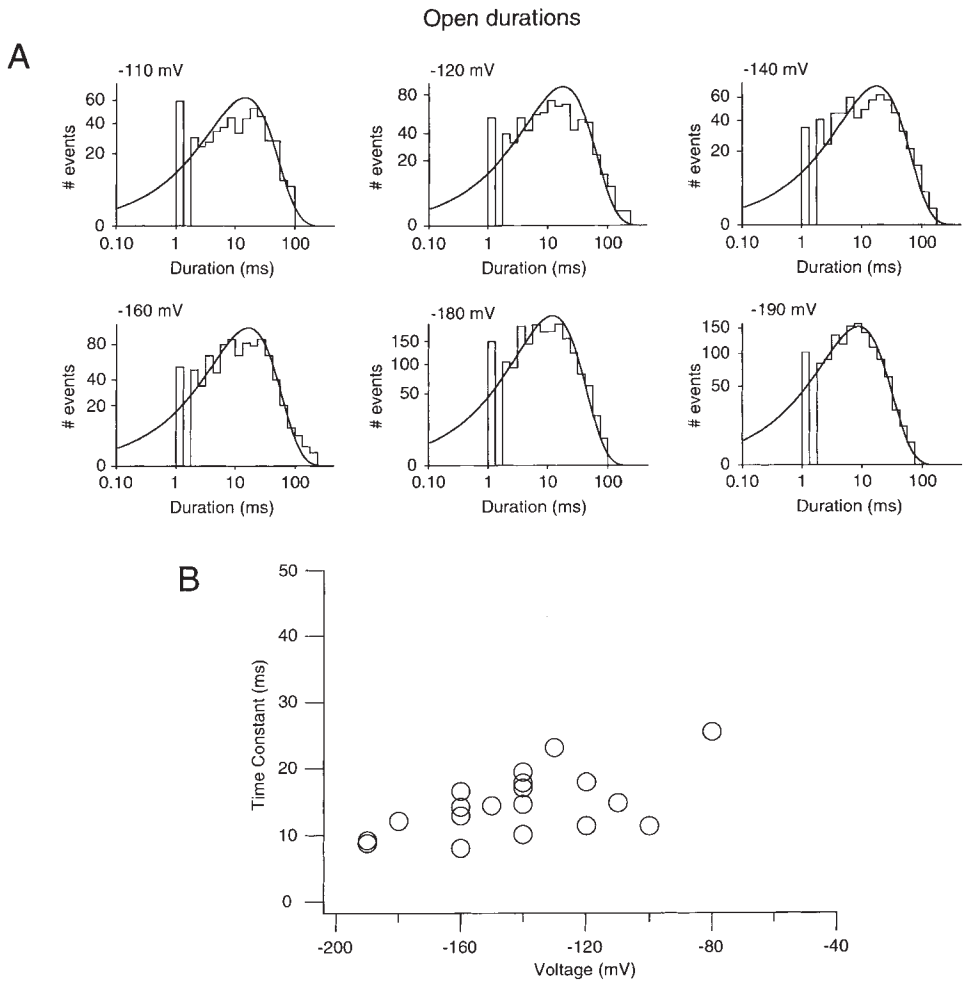

FIGURE 5. (*A*) Frequency histograms of open durations measured at several voltages from KAT1 channels. The data were fitted with single exponential functions, represented by the solid curves. The histograms are plotted using the log-binning transformation of Sigworth and Sine (1987) as described in METHODS. (*B*) Time constants derived from the exponential fits to the open time distributions are plotted as a function of voltage. The data points represent several patches. The exponential fits have been corrected for the left and right censor times, as described in METHODS.

burst analysis. In burst analysis, observed closed events are assigned to one of two kinetically distinguishable closed states using a burst criterion. Closed events longer than the burst criterion are considered closures into an interburst closed state, while closed events shorter than the burst criterion are designated as closures into a within-burst closed state. A burst is then defined as any series of open and closed events for which the closed events are all shorter than the burst criterion. However, it must be noted that any method used to classify closed events as either within-burst or interburst closed events will necessarily misclassify a small fraction of long within-burst closed events as interburst events and a small fraction of short interburst closed events as within-burst events.

The selection of an appropriate burst criterion will minimize false classification of closed events into the inappropriate closed-time distribution (Jackson et al., 1983), and several methods have been described to determine an appropriate burst criterion for a given data set (Magleby and Pallotta, 1983). The method used in this article is to examine the closed-time distributions and select a burst criterion that produces reasonable exponential distributions for both the within-burst closed times and the interburst closed times. A burst criterion of 20 ms was chosen for KAT1, approximately four to five times faster than the brief component time constant of the closed-time distributions. Variation of the burst criterion in this range will not alter the final conclusions derived from the burst analysis, but will alter the specific values of rate constants in the kinetic model by only a modest amount (~20–25% with variation of the burst criteria from 10 to 50 ms).

In Fig. 7 *A*, the distribution of interburst closed times at voltages ranging from −110 to −190 mV are shown. An important limitation of burst analysis is that the distribution of interburst closed times is a valid measure of transitions outside the burst event only if true single channel patches are used, as is the case in Fig. 7. A second limitation to the utility of the interburst closed-time data is that the time constants measured are sensitive to the pulse duration used, as some interburst durations span the pulse duration after the initial burst event and are cut short (the right censor time). This

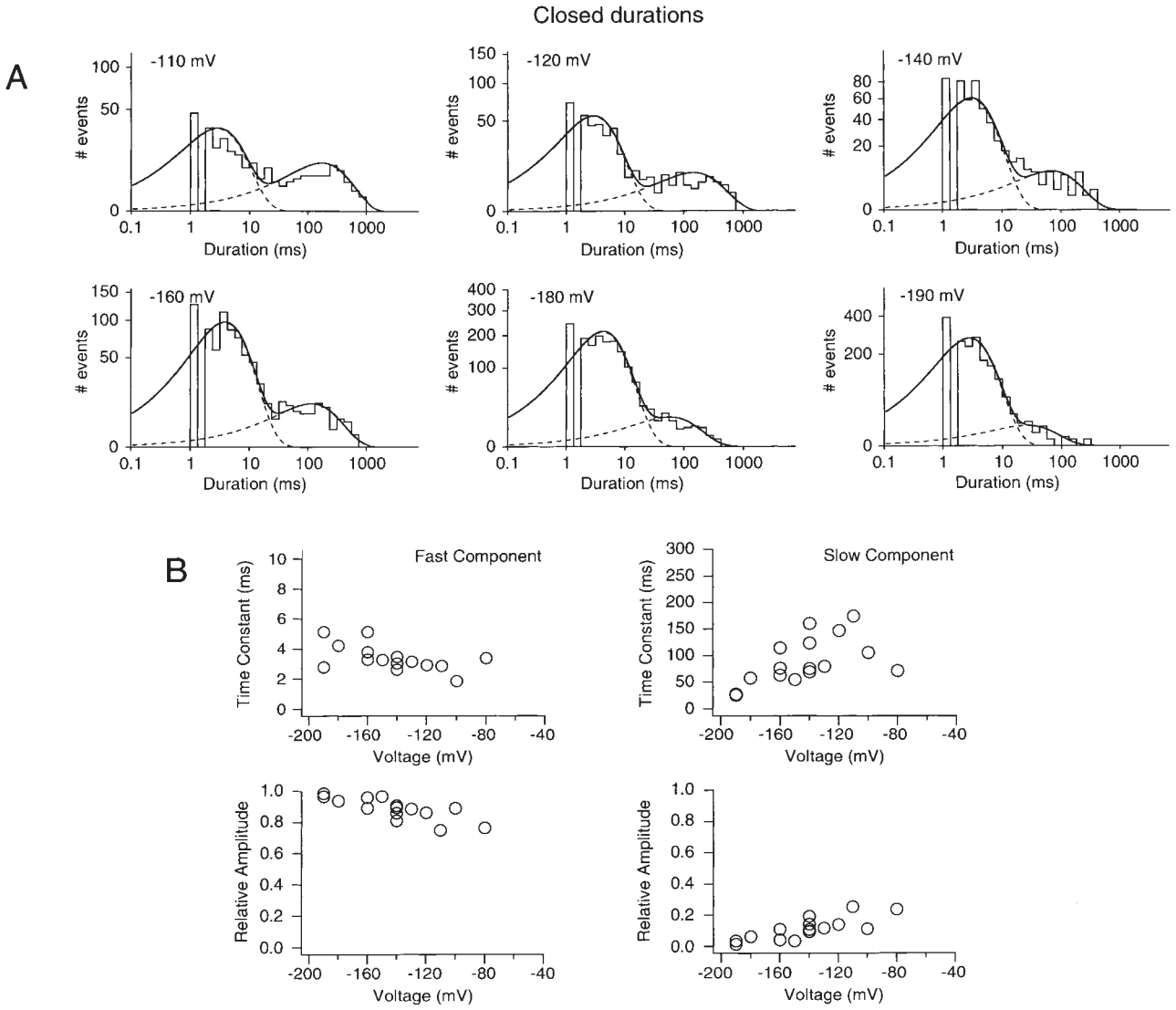

FIGURE 6. (*A*) Frequency histograms of closed-time durations measured at several voltages from KAT1 channels. The data were fitted with a sum of two exponential functions and displayed as described in METHODS. The solid curves represent the overall fits, and the dashed curves represent the individual exponential components. (*B*) The time constants and relative amplitudes for the brief and long components of the fits to closed time distributions are plotted as functions of voltage.

right censor time error was corrected in the exponential fits to the duration distributions (Lawless, 1982; Hoshi and Aldrich, 1988). Fig. 7 *B* plots the time constants from fits to interburst closed-duration distributions as a function of voltage. The interburst closed durations become shorter with increasing hyperpolarization, implying that the channel will spend less time outside of the bursting states with increasing hyperpolarization. The voltage dependence of interburst closed times suggests that the interburst closed-to-open–state transition will proceed in the same direction as overall channel activation, as this transition becomes faster with hyperpolarization. This is most parsimoniously accomplished with a model that places the interburst closed state along the activation pathway, leading directly to the open state. Since it was argued earlier that at least one of the burst closed states is likely to lie outside of the activation pathway, the within-burst closed state will therefore reside outside of the activation pathway in the final kinetic model.

Fig. 8 *A* shows the distribution of within-burst closed times at voltages ranging from −110 to −190 mV. Each distribution has been fitted by a single exponential function, and the time constants from these fits are plotted as a function of voltage in Fig. 8 *B*. There is very little voltage dependence to the within-burst closed times, and because this transition lacks significant voltage dependence, conclusions about the location of the

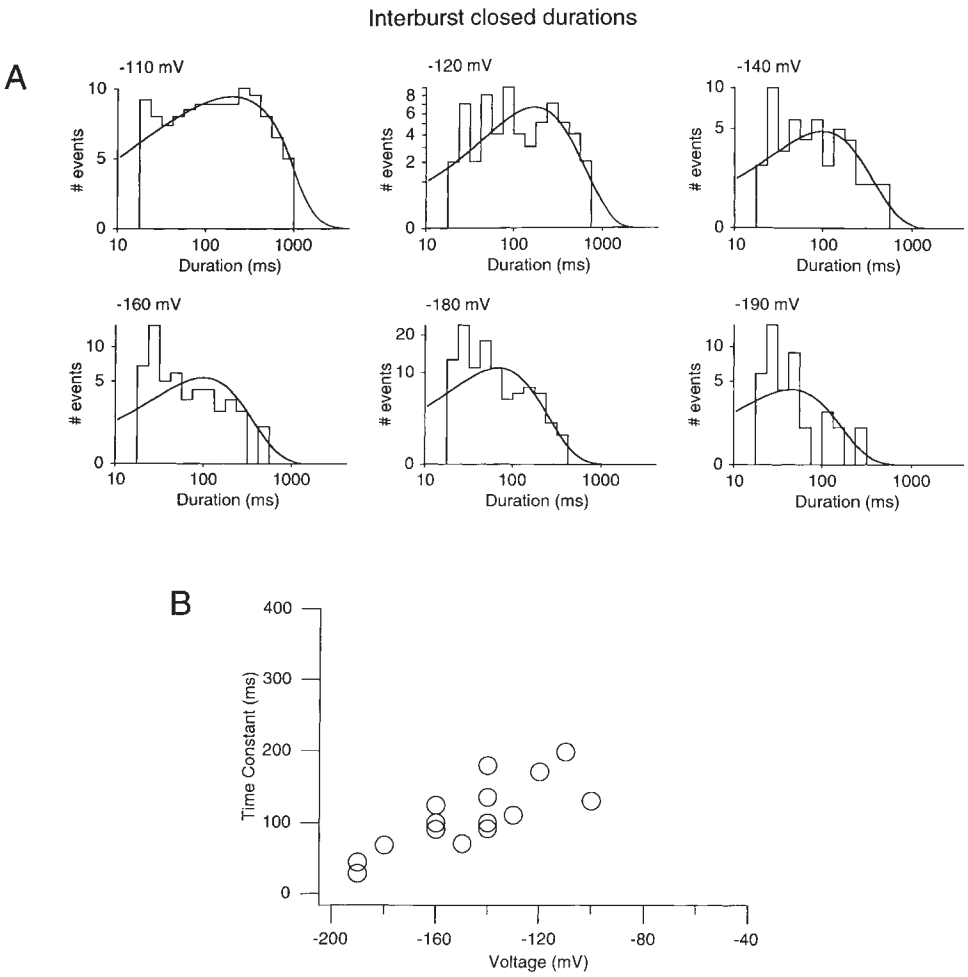

FIGURE 7. (*A*) Frequency histograms of interburst closed durations measured at several voltages from KAT1 channels. The data have been fitted with single exponential functions, represented by the solid lines. (*B*) The interburst duration distribution time constants derived from the single exponential fits are plotted as a function of voltage.

within-burst closed state along the activation pathway cannot be inferred. However, as stated earlier, the within-burst closed state is likely to reside after the open state in the final kinetic model.

A Kinetic Model of KAT1 Gating: Burst Analysis

A kinetic scheme that incorporates bursting behavior will contain at least three kinetically distinguishable states: two closed (the interburst and within-burst closed states) and one open state. With two closed states and one open state, there are exactly three possible configurations for arranging these states with respect to each other. The first is a triangular arrangement, where each of the three states can be entered from any of the two other states directly. This configuration was not entertained because (*a*) there is no experimental evidence in the voltage dependence of the duration distributions that favors a triangular configuration over a linear configuration, and (*b*) such a configuration introduces an additional free parameter into the model. The second configuration is a "CCO" model, as shown in Scheme III, where the two closed states are adjacent and only the shorter-lived closed state is in direct communication with the open state (the bursting states are outlined by the box).

$$C_2 \underset{k_{32}}{\overset{k_{23}}{\leftrightarrow}} \boxed{C_3 \underset{k_{43}}{\overset{k_{34}}{\leftrightarrow}} O_4} \quad \text{Burst}$$

(SCHEME III)

The third configuration is a "COC" model, as shown in Scheme IV, where the open state resides in between the two closed states, allowing direct communication between the open state and both closed states.

$$C_2 \underset{k_{32}}{\overset{k_{23}}{\leftrightarrow}} \boxed{O_3 \underset{k_{43}}{\overset{k_{34}}{\leftrightarrow}} C_4} \quad \text{Burst}$$

(SCHEME IV)

Note that the numbering system used for the states and transitions in Schemes III and IV are labeled to be consistent with the final kinetic scheme determined

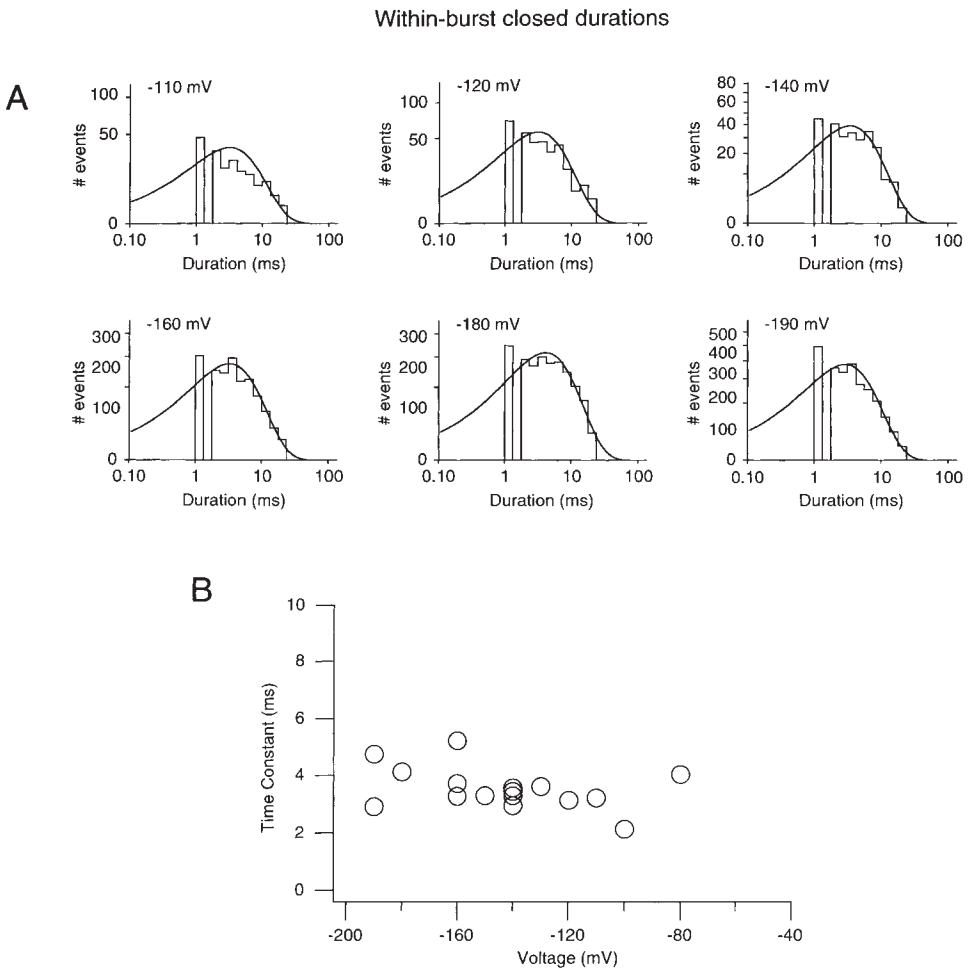

FIGURE 8. (*A*) Frequency histograms of within-burst closed durations measured at several voltages from KAT1 channels. A burst criterion of 20 ms was used. The solid lines represent single exponential fits to the data. (*B*) Time constants derived from the exponential fits to the within-burst closed time duration histograms are plotted as a function of voltage.

later. At any given voltage, it is not possible to discriminate experimentally the CCO and COC models, as both can be fitted equally well to any single channel bursting data set. However, several factors favor the COC model for KAT1 channels. First, given a single open state, as proposed for KAT1, the distribution of open times will be a single exponential with a mean duration of 1/(the sum of all rates leaving the open state). Given the observation that (*a*) KAT1 activation kinetics become faster with increasing hyperpolarization, and (*b*) the sum of leaving rates from the open states also becomes faster with increasing hyperpolarization (Fig. 5 *B*), at least one of the transitions from the open state will likely lie outside the activation pathway, as suggested earlier. Therefore, the minimal kinetic scheme that accounts for both the voltage dependences of these transitions as well as the channel's bursting behavior is most likely the COC scheme. A counter-argument might be that the data can be explained by a CCO or COC bursting model where both burst closed states reside outside the activation pathway, as shown in Scheme V, *A* and *B*, respectively.

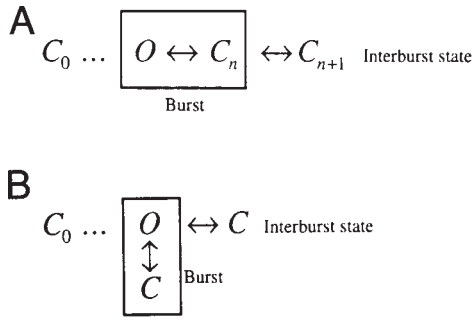

(SCHEME V)

These models are less favorable because they require the introduction of additional states and would also require the voltage dependence of rate constants leaving the interburst closed state to be opposite the voltage dependence of overall activation. Kinetic models as depicted in Scheme V will have more than the minimal number of free parameters necessary to describe the behavior of KAT1 channels. Therefore, a within-burst closed state residing after the open state is the simplest kinetic model to satisfy a COC configuration.

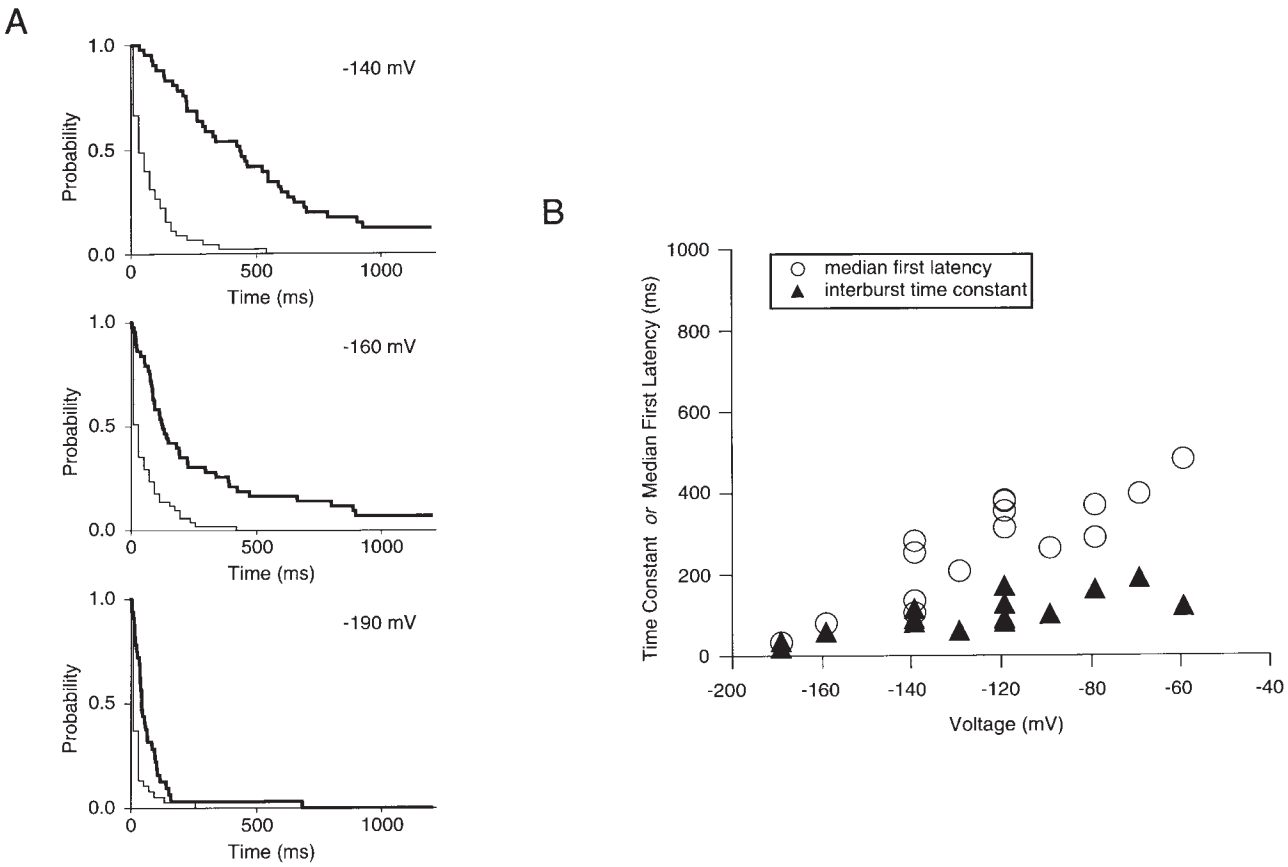

FIGURE 9. (*A*) Comparison of interburst closed durations (*thin lines*) and first latency (*thick lines*) distributions plotted as tail distributions at −140, −160, and −190 mV. The distributions represent the probabilities that the interburst and first latency durations are longer than the times indicated on the axis. (*B*) Mean interburst closed durations and mean first latencies are plotted together as functions of voltage.

If the interburst closed state were indeed to lie within the activation pathway, then the distribution of interburst closed times must be shorter than the distribution of first latencies at any given voltage, as sojourns into the interburst closed state will include a subset of all possible states along the activation pathway. In Fig. 9 *A*, the interburst durations are displayed as tail distributions and superimposed with the first latency tail distributions at −140, −160, and −190 mV. For a population of sweeps at a given voltage, the interburst durations are indeed shorter than the first latencies, consistent with a model that has the interburst closed state located within the activation pathway. The consistently longer distributions for first latencies compared with the interburst closed times also implies that there are multiple closed states along the activation pathway. Moreover, if the interburst closed state were to reside within the activation pathway, then the overall voltage dependence of the interburst closed durations must always be less than or equal to that of the voltage dependence of first latencies. Fig. 9 *B* superimposes the mean interburst closed durations with the mean first latencies as functions of voltage, confirming this prediction.

Therefore, the KAT1 kinetic scheme will at this point have the following features: (*a*) bursting behavior that is described by a COC model, (*b*) a within-burst closed state that lies outside the activation pathway and whose entering rate from the open state becomes faster with increasing hyperpolarization, (*c*) an interburst state that lies within the activation pathway with a transition into the open state that becomes faster with hyperpolarization, (*d*) a relatively voltage-independent transition from the within-burst closed state to the open state, and (*e*) a transition from the open state to the interburst closed state that becomes slower with hyperpolarization. Scheme VI satisfies these criteria.

$$C_0 \ldots C_2 \underset{k_{32}}{\overset{k_{23}}{\leftrightarrow}} \boxed{O_3 \underset{k_{43}}{\overset{k_{34}}{\leftrightarrow}} C_4} \quad \text{Burst}$$

(SCHEME VI)

Using the COC model (Scheme IV) and the general Markov property that the mean dwell time in any particular kinetic state is equal to the inverse of the sum of

all rate constants leaving that state, we can now use the single channel data to assign specific rate constants to transitions in this bursting scheme. Using Scheme IV, the mean open time (Fig. 5) can be described by a single exponential function with a time constant equal to the inverse of the sum of the rates leaving the open state:

$$\tau_{open} = \frac{1}{k_{32} + k_{34}}. \quad (3)$$

The within-burst closed-time distribution is described by a single exponential function with a time constant equal to:

$$\tau_{burstclosed} = \frac{1}{k_{43}}. \quad (4)$$

The interburst closed-time distribution can be described by an exponential function with a time constant as follows, assuming that any other transitions out of this state are negligible:

$$\tau_{interburst} \cong \frac{1}{k_{23}}. \quad (5)$$

Note that Eq. 5 is an approximation if Scheme VI is entertained, as it assumes that all long closed events after first opening only involve transitions into the interburst state without additional transitions into adjacent closed states along the activation pathway. This is a reasonable assumption at the hyperpolarized potentials studied, where the interburst closed-time distributions are well fitted with single exponentials and the backward rates away from the bursting states are expected to be relatively slow.

Furthermore, according to Scheme IV, an open channel will continue to burst with a probability of

$$\frac{k_{34}}{k_{32} + k_{34}},$$

and it will terminate a burst with a probability of

$$\frac{k_{32}}{k_{32} + k_{34}}.$$

The number of openings per burst (n) will be described by a geometric distribution:

$$P(n) = (1 - q)^{n-1} q, \quad (6)$$

where

$$q = \frac{k_{32}}{k_{32} + k_{34}}$$

is the probability of terminating a burst. The distribution described by Eq. 6 gives a mean number of openings per burst equal to

$$\overline{m_o} = 1 + \frac{k_{34}}{k_{32}}.$$

In Fig. 10 *A*, the distributions of the number of openings per burst are shown for voltages ranging from −110 to −190 mV. The distributions of the number of openings per burst are fitted with geometric distributions, and the probability of terminating a burst (q) derived from these fits are plotted as a function of voltage in Fig. 10 *B*. Eqs. 3–6, along with measurements of open time, closed time, and burst durations over a wide voltage range can then be used to determine every rate constant of Scheme IV by solving for each individual rate constant as a function of the various measured dwell time distributions. In Table I, the equations for determining each rate constant in the COC bursting scheme are shown.

The interburst closed-duration distributions were not as well determined as the other distributions because of the relatively small number of events in each distribution. Therefore, the associated rate constant (k_{23}) was allowed to relax in fitting the ensemble averages and cumulative first latency distributions (see below). However, the final values determined for this rate constant are comparable with the original values determined by burst analysis. The calculated burst rate constants are plotted as functions of voltage in Fig. 11 *A*. As expected, the forward rate constants k_{23} and k_{34} become faster with increasing hyperpolarization, while the rate constant leaving the burst (k_{32}) becomes slower with increasing hyperpolarization. The rate constant leaving the within-burst closed state (k_{43}) is essentially voltage independent. Interestingly, the two individual rate constants leaving the open state demonstrate relatively strong voltage dependence, but because their voltage dependences are in opposite directions, the open time distributions are much less voltage dependent. Moreover, all four rate constants appear to follow a single exponential voltage dependence.

TABLE I

Formulas Used to Calculate Burst Transition Rates

Rate	Solution
k_{23}	$k_{23} = \frac{1}{\tau_{interburst}}$
k_{34}	$k_{34} = \frac{(1-q)}{\tau_{open}}$
k_{32}	$k_{32} = \frac{q}{\tau_{open}}$
k_{43}	$k_{43} = \frac{1}{\tau_{burstclosed}}$

Equations for the individual rate constants in the bursting model of Schemes IV and VIII. The equations were derived by solving for each rate constant in Eqs. 3–6. To solve for rate constants k_{34} and k_{32}, Eq. 3 describing the mean open duration was solved simultaneously with the equation describing the probability of terminating a burst:

$$q = \frac{k_{32}}{k_{32} + k_{34}}.$$

The interburst closed duration distributions were not as well determined as the other bursting parameters because each distribution had significantly fewer data points. Therefore, the rate constant k_{23} as determined by burst analysis was allowed to relax when fitting the ensemble averages and first latency distributions.

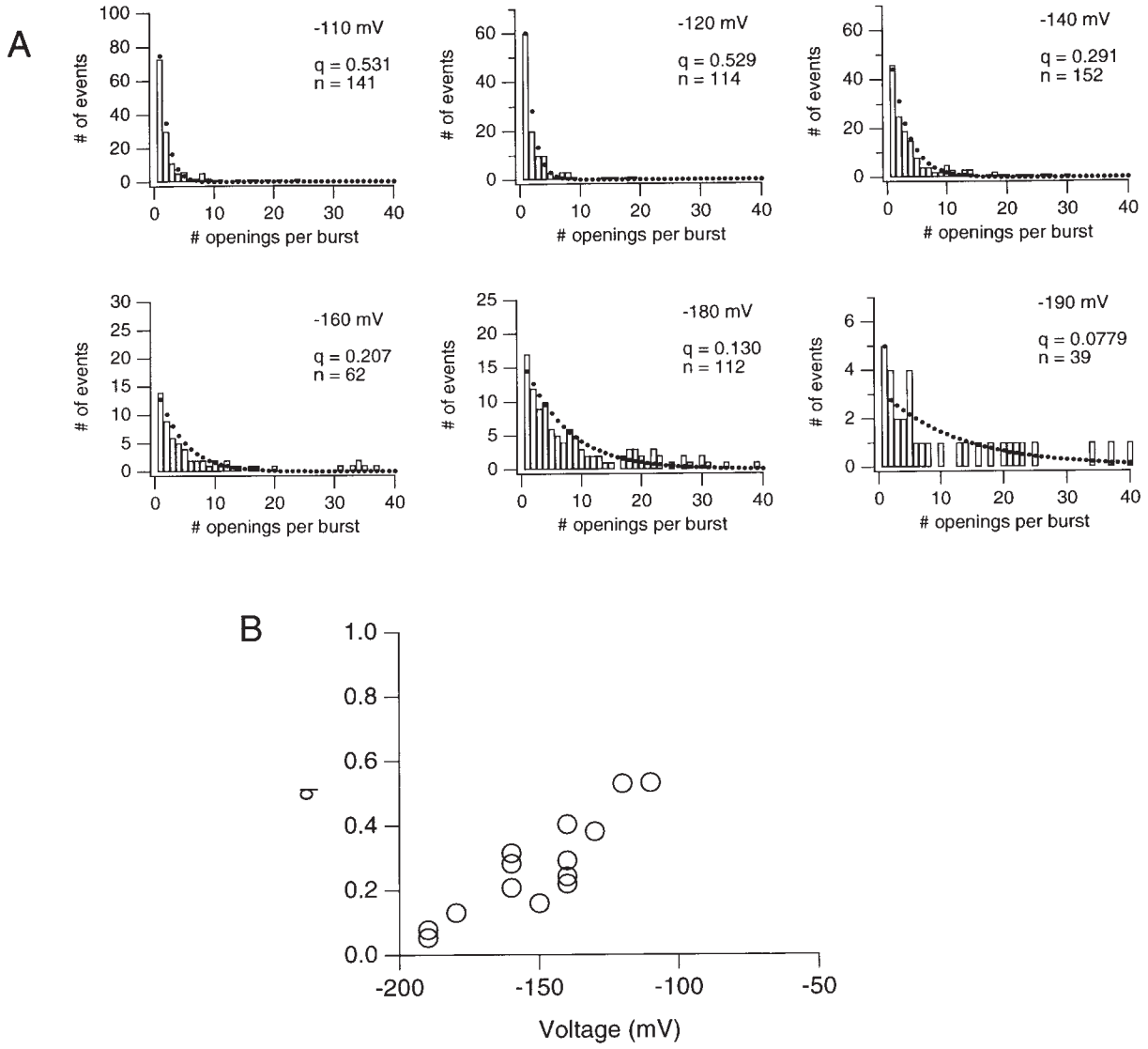

FIGURE 10. (*A*) Frequency histograms of the number of openings per burst at several voltages, using a burst criterion of 20 ms. The data are fitted by a geometric distribution (Eq. 6), represented by the dots. The probability of terminating a burst (q) and the total number of openings are shown for each voltage. (*B*) The probability of terminating a burst (q), derived from the geometric fits, is plotted as a function of voltage.

As stated earlier, the probability of terminating a burst (q) decreases significantly with more negative voltages, suggesting that the channel is more apt to continue bursting at hyperpolarized potentials. Moreover, this voltage dependence of q is consistent with the interburst closed state residing within the activation pathway and the within-burst closed state residing outside of the activation pathway. These data also imply that the increased steady state open probability with more negative voltages is in large part a result of longer bursting periods. This can be confirmed by examining the distribution of burst durations. The mean burst duration can be measured directly and calculated from the rate constants determined in Scheme IV, as follows. The product of the mean number of openings per burst and the mean open time will give the total time a channel spends in the open state per burst:

$$T_{\text{burstopen}} = \overline{m_o} \times \tau_{\text{open}} = \left(1 + \frac{k_{34}}{k_{32}}\right)\left(\frac{1}{k_{32} + k_{34}}\right) = \frac{1}{k_{32}}.$$

Likewise, the total time spent per burst in the within-burst closed state is the product of the mean within-burst closed time and the mean number of openings per burst, less one:

$$T_{\text{burstclosed}} = (\overline{m_o} - 1) \times \tau_{\text{burstclosed}} = \frac{k_{34}}{k_{32}k_{43}}.$$

The mean burst duration is then the sum of the mean total open and closed times per burst:

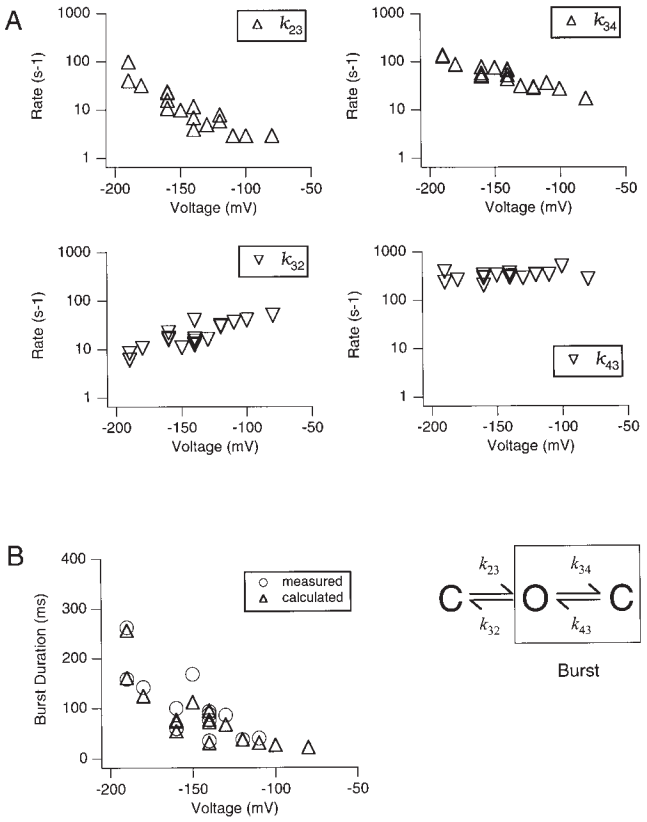

FIGURE 11. (*A*) The rate constants k_{23}, k_{34}, k_{32}, and k_{43} from Scheme IV, calculated using Eqs. 3–6, are plotted as functions of voltage. The voltage dependences of the four rate constants are plotted on logarithmic scales. (*B*) Comparison of the mean burst durations measured directly using a burst criterion of 20 ms (○) and calculated using Eq. 7 and the rate constants derived from burst analysis (△). The COC bursting scheme is shown at right for reference.

$$\overline{T}_{\text{burstduration}} = T_{\text{burstopen}} + T_{\text{burstclosed}} = \frac{k_{34} + k_{43}}{k_{32}k_{43}}. \quad (7)$$

Fig. 11 *B* superimposes the measured mean burst durations and the mean burst durations calculated by applying the rate constants in Fig. 11 *A* to Eq. 7 as functions of voltage, which serves as an internal check for correctness of fit and theory. Fig. 11 *B* demonstrates close agreement between the measured and calculated burst durations, confirming that Scheme IV describes the bursting behavior of KAT1 reasonably well.

A Kinetic Model of KAT1 Gating

The nucleus of a kinetic model for KAT1 gating can be described by Scheme IV, with rate constants derived from burst analysis (Fig. 11 *A*). The next step in creating a kinetic model is to account for the behavior of the KAT1 channel before first opening. This model will have the following properties: (*a*) a COC bursting scheme as described in the previous section, (*b*) any additional closed states in the activation pathway will be located to the left of the interburst closed state, as shown earlier in Scheme VI, and (*c*) the voltage dependence of each rate constant is assumed to be in the same direction as the overall voltage dependence of the KAT1 channel, where increasing hyperpolarization produces faster rates in the general direction of activation (left-to-right in Scheme VI) and slower rates in the reverse direction (right-to-left in Scheme VI).

The number of closed states in the activation pathway and the values and voltage dependences of their rate constants must account for the first latency and ensemble average data. Macroscopic currents, ensemble averages, and first latency distributions all display a small but measurable sigmoidicity in the activation time course that must be incorporated in the model. Fits of the data to several candidate models suggest that a minimum of three closed states, including the interburst closed state, are located along the activation pathway. Furthermore, the transition from the interburst closed state to the open state is not a free parameter at this point, as its values in the voltage range of KAT1 activation have been determined by the burst data. Fewer than three closed states in the activation pathway failed to produce adequate fits to the ensemble average and first latency data (data not shown). The minimal configuration necessary to account for these data is shown in Scheme VII.

$$C_0 \underset{k_{10}}{\overset{k_{01}}{\leftrightarrow}} C_1 \underset{k_{21}}{\overset{k_{12}}{\leftrightarrow}} C_2 \underset{k_{32}}{\overset{k_{23}}{\leftrightarrow}} \boxed{O_3 \underset{k_{43}}{\overset{k_{34}}{\leftrightarrow}} C_4} \quad \text{Burst}$$

(SCHEME VII)

Inactivated States

As discussed previously, the first latency distributions (Fig. 3 *A*) do not always reach a steady state probability of one, reflecting either an inactivated state entered directly from one of the closed states, right-censoring of the data, or incomplete recovery from closed or inactivated state(s) entered after the channel opens. To produce good qualitative fits to the steady state open probabilities derived from ensemble averages and the distributions of first latencies in the positive voltage range, a transition to an inactivated state directly entered from state C_0 was introduced. The contribution of blank sweeps is significant only at depolarized potentials. The minimal contribution of the inactivated state was determined to be the contribution required to account for steady state cumulative first latencies less than one in the fits not accounted for by first latencies longer than the right censor time. This small correction can then be incorporated into the model as an inactivated or accessory closed state that is entered directly from the closed state(s) along the activation

pathway. In our analysis, only the minimal contribution of the inactivated state has been determined.

Although inactivation could, in principle, occur from a number of closed states, state C_0 in Scheme VII was chosen as the state connected directly with the inactivated state for several reasons. First, among the closed states along the activation pathway, locating the inactivated state at state C_0 is least likely to affect the burst kinetics previously described, which do not suggest the existence of an inactivated state near the burst states. Second, it is unlikely that the inactivated state can be entered either from the open state (O_3) or the closed state located outside the activation pathway (C_4). Given the fraction of blank sweeps observed at depolarized voltages and given the fit of Scheme VII to the activation kinetics and burst data, the rate constant required for entering an inactivated state located in direct connection with either states O_3 or C_4 would result in an observable time-dependent inactivation process in the ensemble averages. Furthermore, this time-dependent inactivation process would only be apparent at depolarized potentials where the entry rate into the inactivated state is significant. A time-dependent inactivation process is not observed in KAT1 ensemble averages (Fig. 2 *A*), which makes such a kinetic scheme unlikely; however, a model in which the inactivated state can be accessed from more than one state along the activation pathway cannot be excluded.

The Final Kinetic Model

Given the rate constants derived for Scheme VII, the observation of blank sweeps in KAT1 currents at depolarized voltages is best accounted for by the combined contribution of first latencies longer than the pulse potential and by an inactivated state that can be directly entered by a closed state(s) located early along the activation pathway (Scheme VIII).

$$\begin{array}{l} C_0 \underset{k_{10}}{\overset{k_{01}}{\leftrightarrow}} C_1 \underset{k_{21}}{\overset{k_{12}}{\leftrightarrow}} C_2 \underset{k_{32}}{\overset{k_{23}}{\leftrightarrow}} \boxed{O_3 \underset{k_{43}}{\overset{k_{34}}{\leftrightarrow}} C_4} \quad \text{Burst} \\ \updownarrow \\ I \end{array}$$

(SCHEME VIII)

In Scheme VIII, the rate of entering the inactivated state is slow at hyperpolarized voltages and fast at depolarized voltages. The recovery rate from this inactivated state is relatively fast at all voltages examined.

Fig. 12 *A* displays fits of Scheme VIII to the ensemble averages at voltages ranging from −110 to −190 mV. Values for the rate constants k_{23}, k_{34}, k_{32}, and k_{43} were those derived from the burst analysis, with the rate constant k_{23} allowed to relax, as mentioned earlier. The same values for all rate constants were used in the fits to the ensemble averages as well as the first latency distributions. The data are well fitted by three closed states in the activation pathway, and the model accounts for the sigmoidicity of activation as well as the voltage dependence of activation. Fig. 12 *B* displays first latency cumulative distributions at voltages ranging from −110 to −190 mV fitted with Scheme VIII. An important assumption made in deriving these fits was that the reverse transitions before first opening are negligible, which is reasonable over the hyperpolarized potentials examined, particularly in the voltage range where the steady state open probability is greater than one half. Therefore, these reverse rate constants were set to zero at all activating potentials measured. Relaxing this constraint does not alter the overall architecture of the kinetic scheme used; rather, using nonzero reverse transitions merely changes the absolute values of the forward rates.

The model's ability to predict the deactivation kinetics and voltage dependence can best be tested by fitting the macroscopic tail currents. Fig. 13 *A* plots a family of tail currents recorded from macroscopic patches between −100 and −10 mV in 10-mV steps elicited after a test pulse to −160 mV. Deactivation tail currents are relatively fast in this voltage range. The tail currents have been fitted with Scheme VIII. The tails were inverted and scaled so that the initial current amplitude would fit the model's prediction of the steady state open probability at −160 mV. Because the test pulse of −160 mV does not maximally activate KAT1 channels according to the open probability voltage dependence in Fig. 2 *B*, the relative distribution of initial probabilities among the various states in Scheme VIII was determined by fits to the model. These fits reveal that the rate constant k_{32} is the most important determinant of the time course of the deactivation tail currents, and, moreover, the values for this rate constant determined by burst analysis predict the deactivation tail kinetics well.

The model also predicts the existence of a small but noticeable initial rising phase that lasts <2 ms during the deactivation tail currents at depolarized potentials. According to the model, transitions from the within-burst closed state (C_4), through the open state (O_3), and then into the interburst closed state (C_2) account for the rising phase seen in the deactivation tail currents. The observed deactivation tail currents were fitted to the predominantly single exponential decaying time course of the model tail currents, and in Fig. 13 *A* the tail currents are shown only after the initial capacitive transient, and so an initial rising phase is not seen. However, the predicted rising phase has been observed in KAT1 deactivation tails when recording conditions are optimized for more rapid kinetic measurements (T. Hoshi, personal communication). The ability of the

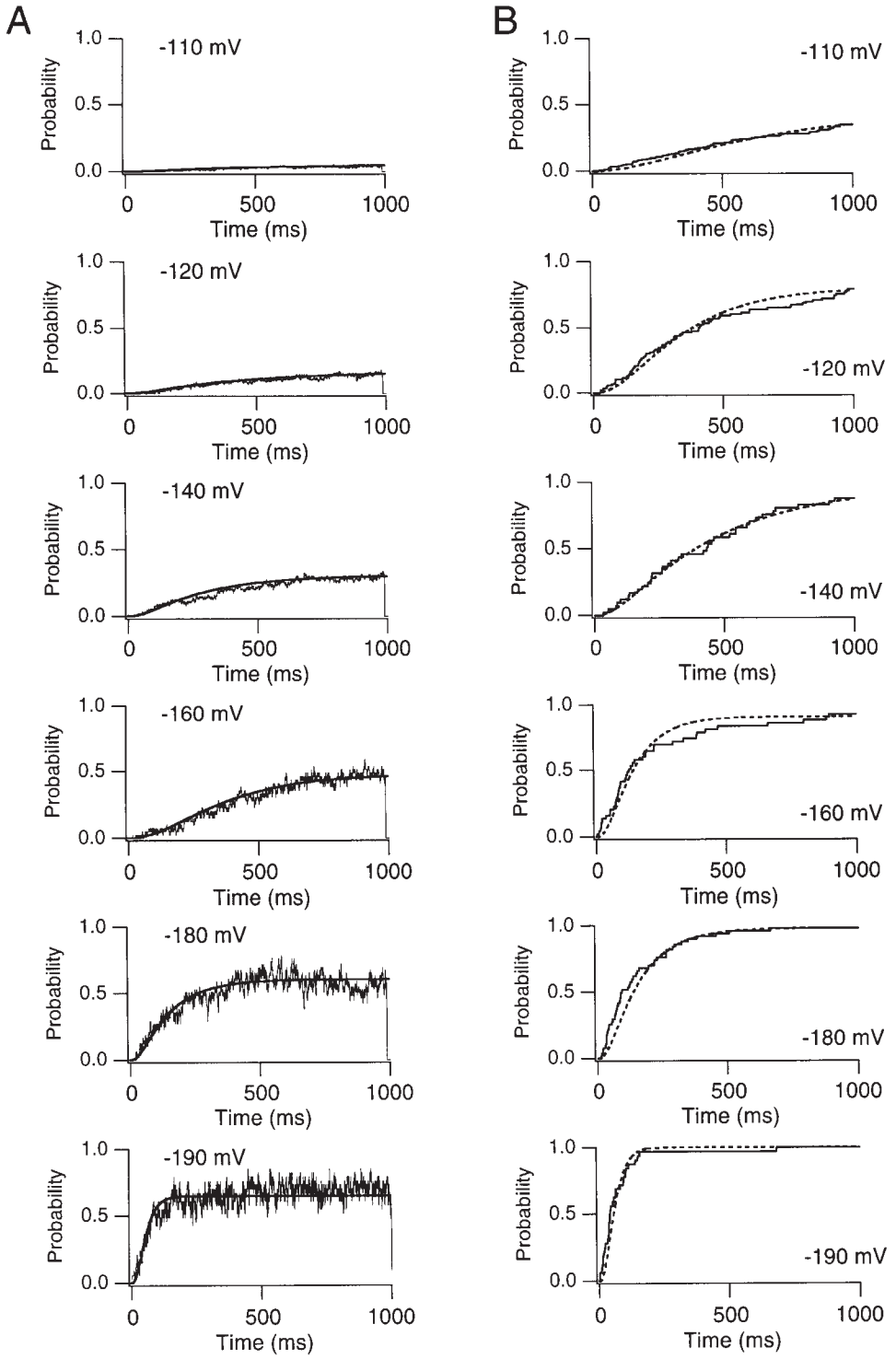

FIGURE 12. (*A*) Fits of Scheme VIII to KAT1 ensemble averages at several voltages. Best fits were determined by eye. The rate constants k_{23}, k_{34}, k_{32}, and k_{43} were determined by the burst analysis as shown in Fig. 19, and the reverse transitions k_{10} and k_{21} were set to zero over the voltage range examined in this figure. The thick, smooth lines represent the fits, while the thin, noisy lines represent the ensemble averages. Voltages are indicated. (*B*) Fits of Scheme VIII to cumulative first latency distributions for KAT1 at several voltages. All rate constants except forward transitions before first opening, k_{01}, k_{12}, and k_{23}, were set to zero over the entire voltage range examined. The solid lines represent the first latencies, and the dashed lines represent the fits.

model to fit the overall macroscopic tail kinetics demonstrates that Scheme VIII can adequately predict the deactivation properties of KAT1. In Fig. 13 *B*, the measured steady state single channel G(V) relationship is compared with the G(V) predicted by the model, demonstrating close agreement.

Evident in the first latency distributions, particularly at voltages ranging from −140 to −160 mV, is a slow component of activation that is not well fitted by Scheme VIII, as noted in fits to first latencies in Fig. 12 *B*, a "slow creep" particularly evident between −120 and −160 mV. This slow creep can be accounted for with a closed state that branches off from one of the closed states along the activation pathway. However, for the purposes of this article, the slow creep was not accounted for in the final kinetic scheme.

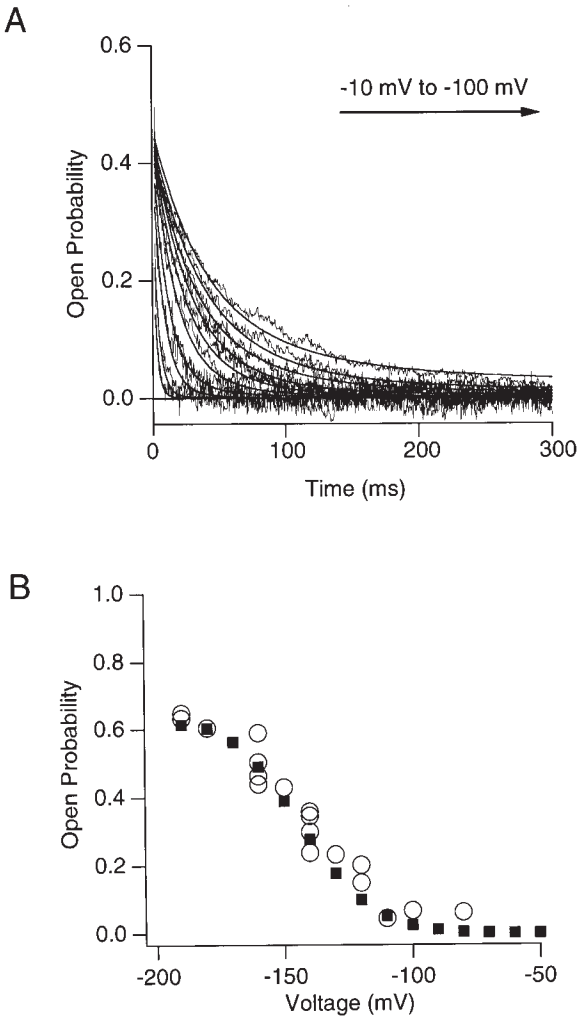

FIGURE 13. (*A*) Fits of KAT1 macroscopic deactivation tail currents to Scheme VIII. The tails were elicited after a 500-ms activating pulse to −160 mV, followed by a 500-ms tail pulse over a voltage range of −100 to −10 mV in 10-mV steps. The tail currents have been reversed in polarity to facilitate fits using the model. The tail currents were scaled at their initial points to coincide with the steady state open probability predicted by the model for the activating potential used (−160 mV). The distributions of initial probabilities among the various states in Scheme VIII were determined by fits of the model to the burst, ensemble average, and first latency data. (*B*) Fits of Scheme VIII to the steady state open probability versus voltage relationship for wild-type KAT1 currents. The steady state open probability (○) was determined as described in Fig. 2. The open probabilities calculated from the model (■) were determined by measuring the steady state open probability from the calculated waveforms.

An additional modification to the kinetic model for KAT1 gating can be considered. Given the structural similarities between KAT1 and *Shaker* K^+ channels, it could be argued that KAT1 channels are likely to be formed by a tetramer of four individual KAT1 subunits, as seen in *Shaker* channels. It is therefore interesting to consider whether KAT1 activation follows a Hodgkin-Huxley (HH) scheme, with four independent and identical transitions that must occur before the channel first opens (Hodgkin and Huxley, 1952), or perhaps a scheme similar to that described for *Shaker* channels involving independent and identical transitions followed by an additional transition before the open state (Zagotta and Aldrich, 1990; Zagotta et al., 1994*b*; Schoppa and Sigworth, 1998*c*). In fits to both the ensemble averages and the first latencies, the HH model and the related model with an additional final transition predicts too much sigmoidicity in the activation time course, particularly at depolarized voltages. Given all of the considerations enumerated so far, it can be argued that the kinetic model described by Scheme VIII best predicts the gating behavior of KAT1 channels among the models considered in this article.

In Fig. 14, the rate constants for every transition described in Scheme VIII are plotted as functions of voltage. Note that the four rate constants described by the burst analysis are identical to those presented in Fig. 11, with only minor alterations in the rate constant k_{23}. Moreover, the specific values determined for rate constants in Scheme VIII do not follow the ratios expected for a Hodgkin-Huxley model, again arguing against such a model. The voltage-dependent rate constants in Fig. 14 have been fitted by single exponential functions using the following equation:

$$k_n = n_0 e^{-z_n (FV)/(RT)}, \qquad (8)$$

where z_n represents the equivalent gating charge. The amplitudes and voltage dependencies, expressed as units of electronic charge, are shown for each rate constant in Table II. The magnitude of the total charge obtained by adding the individual equivalent charges for each rate constant in Scheme VIII is 3.42e, while the

TABLE II

Summary of the Fits to the Rate Constants for Scheme VIII

Rate constant	n_0 (s^{-1})	z_n (e^- charges)
k_{01}	11.8	0.24
k_{12}	1.17	0.26
k_{23}	0.24	0.71
k_{34}	3.67	0.47
k_{10}	139	−0.57
k_{21}	126	−0.71
k_{32}	186	−0.40
k_{43}	430	−0.056

Amplitude and equivalent charge derived from exponential fits to the rate constants in Scheme VIII. Each rate constant has been fitted with a single exponential function: $k_n = n_0 e^{-z_n FV/RT}$ where V is voltage, and *F*, *R*, and *T* have their usual meanings. The absolute value of the total equivalent charge derived by summation of all individual charges from each rate constant is 3.42e, compared to an absolute value of the apparent charge of 1.36e derived by the Boltzmann fit to the G(V) relationship. In general, the rate constants closer to the open state are more important in determining the quantitative fits to the data, and are therefore better determined than the other rate constants.

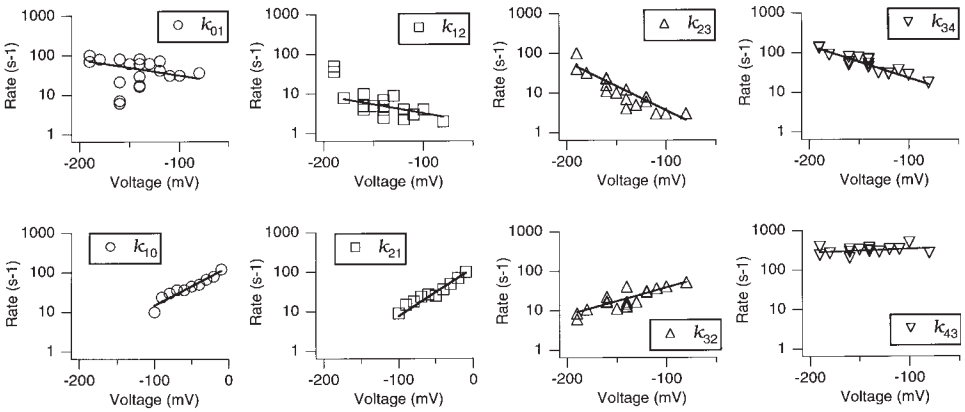

FIGURE 14. Rate constants for Scheme VIII are plotted as functions of voltage. The rate constants k_{23}, k_{34}, k_{32}, and k_{43} were determined by burst analysis as shown, while the rate constants k_{01} and k_{12}, and the final value for k_{23} were determined by fits of the model to the first latency and ensemble averages, given the rate constants determined by burst analysis in the COC model. The rate constants k_{10} and k_{21} were set to zero over the activation voltage range between −110 and −190 mV, and fits of the model to macroscopic deactivation tail currents were used to determine these rate constants between −100 and −10 mV. Several patches are represented by the data points.

magnitude of the apparent charge derived from fitting the G(V) relationship is 1.36e. This discrepancy highlights the caution required in interpreting parameters obtained from fits of the data to a Boltzmann function when the appropriate gating scheme is not a simple two-state model.

Mutations in the S4 Region

Mutagenesis studies of the S4 region of *Shaker*-family potassium channels have implicated the S4 region in voltage-dependent gating (Liman et al., 1991; Papazian et al., 1991; Logothetis et al., 1992, 1993; Schoppa et al., 1992; Tytgat and Hess, 1992; Shao and Papazian, 1993; Yang and Horn, 1995; Larsson et al., 1996; Mannuzzu et al., 1996; Cha and Bezanilla, 1997). Given these results, one might expect that similar mutations in the S4 region of KAT1 would also have substantial effects on voltage-dependent gating, if indeed the gating mechanisms of KAT1 bear structural and mechanistic similarities to that of other voltage-gated channels. Initially, several neutralization mutations in the S4 region of KAT1 were introduced (our unpublished results), and a wide range of effects was seen on voltage-dependent gating. The two mutations with the most dramatic effects, R177Q and R176L, were chosen for further study using single channel kinetic analysis. In Fig. 15, the S4 sequence of wild-type KAT1 is shown along with the R177Q and R176L mutations.

Fig. 16 compares representative single channel current sweeps from wild-type KAT1 (*left*), R177Q mutant (*center*), and R176L mutant (*right*) channels. Voltages encompassing the range of activation were used for all three channels. The voltage range of activation for both R177Q and R176L is much more positive than that of wild-type KAT1 channels. However, the wild-type and two mutant KAT1 channel currents have several characteristics in common, including voltage-dependent first latencies and bursting behavior. Neither S4 mutation altered single channel conductance.

The overall behavior of the two S4 mutant channels can be examined with ensemble averages. Fig. 17, *A* and *B*, plots ensemble averages expressed as open probabilities over a range of voltages for the R177Q and R176L mutants. In Fig. 17, *C* and *D*, the steady state open probabilities are plotted as a function of voltage. For comparison, the open probability–voltage relationship for wild-type KAT1 is plotted simultaneously. Overall, these S4 mutations shift the equilibrium between the open and closed states towards the open state over the activation voltage range. Fits to a Boltzmann function (Eq. 2) for both S4 mutations demonstrate depo-

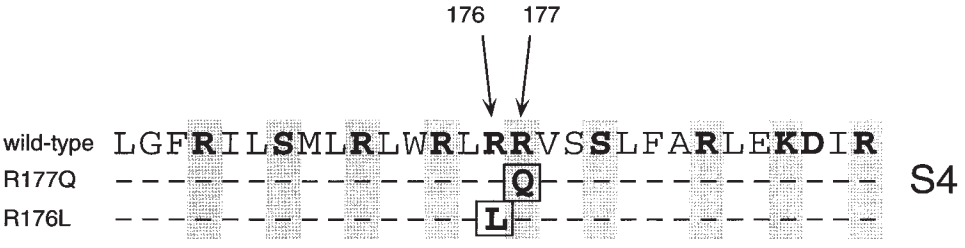

FIGURE 15. Amino acid sequences of wild-type KAT1, R177Q, and R176L mutant channels. The charged amino acid residues at every third position are highlighted, and the mutated residues are shown below the wild-type KAT1 S4 sequence.

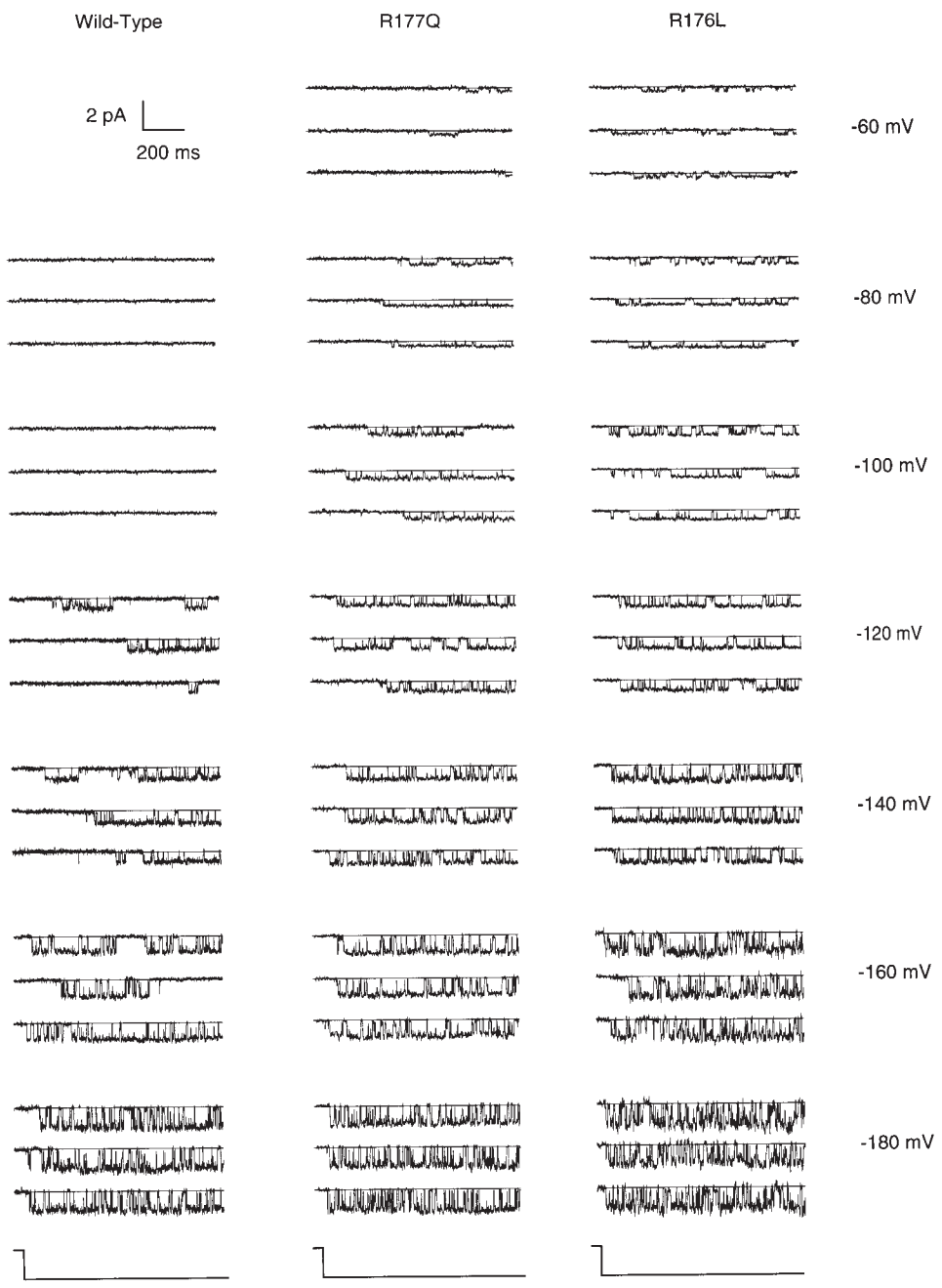

FIGURE 16. Representative single channel currents from wild-type KAT1 (*left*), R177Q (*middle*), and R176L (*right*) channels recorded in the inside-out patch configuration in response to hyperpolarizing voltage pulses. The voltages are indicated. The data for wild-type KAT1 at all voltages shown were filtered at 0.6 kHz and sampled at 1.54 kHz, and are the same traces as shown in Fig. 1. The data for R177Q at −180, −160, −140, −120, −100, −80, and −60 mV were filtered at 0.6, 0.6, 0.7, 0.7, 0.7, 0.2, and 0.15 kHz, respectively, and sampled at 0.95 kHz. The data for R177Q at −180, −160, −140, −120, −100, −80 and −60 mV were filtered at 0.9, 0.9, 0.3, 0.5, 0.4, 0.4, and 0.15 kHz, respectively, and sampled at 0.95, 0.95, 0.95, 1.54, 1.54, 1.54, and 0.95 kHz, respectively. The voltage pulses were delivered every 2–6 s. The prepulse, tail, and holding potentials were −40 mV for wild-type currents and 0 mV for both R177Q and R176L currents.

larizing shifts in the $V_{1/2}$ compared with wild-type KAT1, by +54 and +89 mV in R177Q and R176L, respectively. The slope factor, z, is unchanged in the R177Q mutant, while R176L decreases the absolute value of the apparent steady state voltage dependence (z = 0.54e, compared with 1.36e in the wild type).

In Fig. 17, *A* and *B*, the ensemble averages have been fitted using Scheme VIII (see below). Note that the early times in the fits to ensemble averages for R176L deviate from the data slightly. This is likely a result of the prepulse potential used in the pulse protocol (0 mV), which is a potential at which the steady state open probability of R176L is not zero. Therefore, a small number of sweeps will have currents from channels that are already open before the start of the voltage pulse. This can be corrected by a small adjustment in the initial probabilities to correspond to the predicted nonzero open probability for R176L (data not shown).

Mutations in the S4 Region: Effects on Closed States Before First Opening

As seen in the ensemble averages for R177Q and R176L in Fig. 17, the time course of activation is faster in the

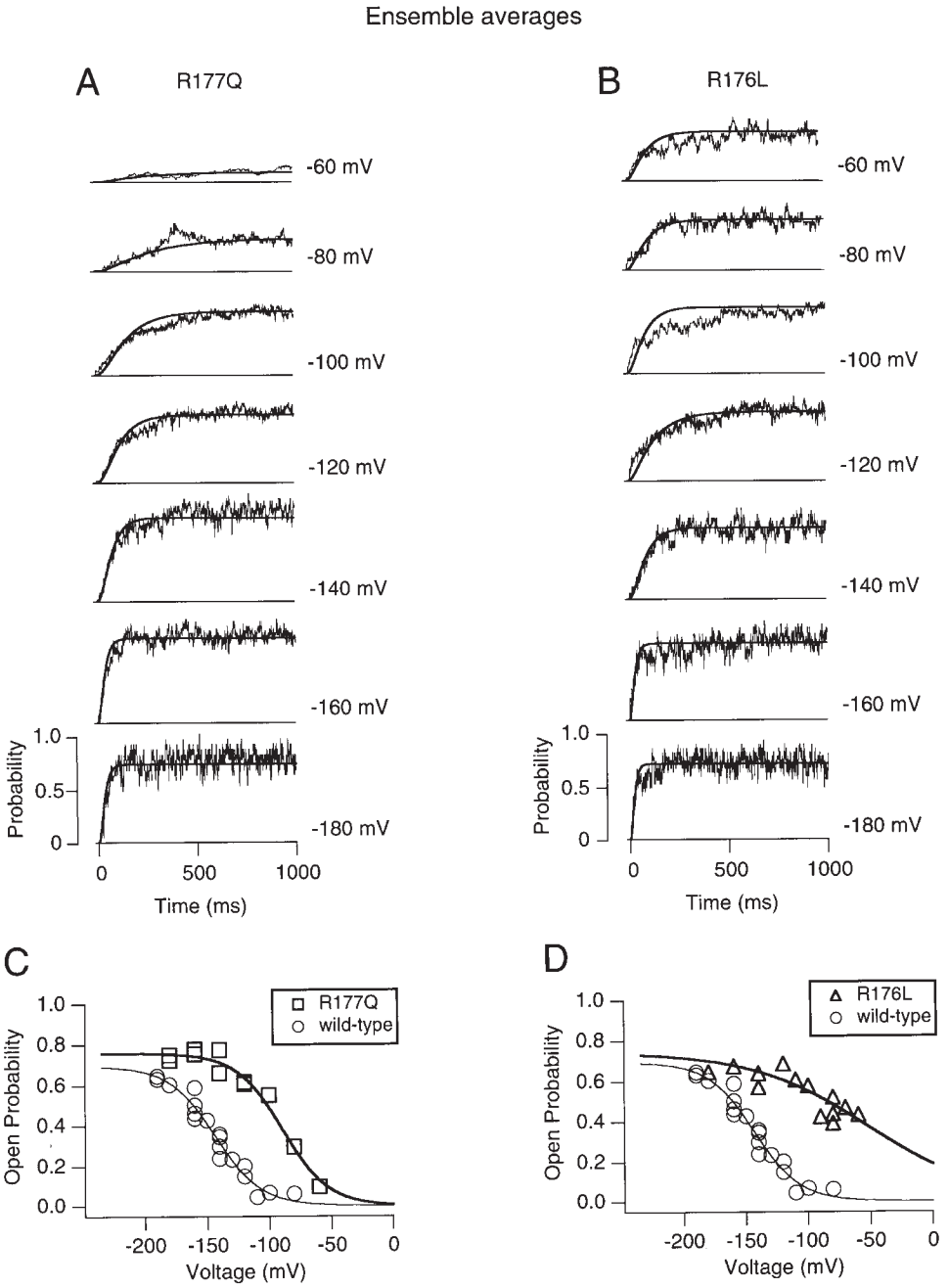

FIGURE 17. (*A*) Ensemble averages of R177Q single-channel currents expressed as open probabilities at several voltages. Open probability is calculated by dividing the ensemble average current by the number of channels in the patch (only single channel patches were used in the ensemble averages shown) and the measured unitary current amplitude. Voltages are indicated. Recording conditions were as described in Fig. 16. Fits of Scheme VIII to the ensemble averages have been superimposed, represented by the solid lines. (*B*) Ensemble averages of R176L single-channel currents expressed as open probabilities at several voltages. Open probability was calculated as described in *A*, and fits to the ensemble averages using Scheme VIII have been superimposed, represented by the solid lines. (*C*) Voltage dependence of the steady state open probability for R177Q single channel currents, with wild-type open probabilities superimposed. Data from several patches are shown. The smooth curves represent Boltzmann functions expressed by Eq. 1. (*D*) Voltage dependence of the steady state open probability for R176L single channel currents, with wild-type open probabilities superimposed. Data from several patches are shown. The smooth curves represent Boltzmann functions as described in *C*.

mutant channels compared with the wild-type channel. In Fig. 18, *A* and *B*, first latencies are plotted as cumulative distributions over a wide voltage range for R177Q and R176L channels, respectively. Fits to the first latency distributions using Scheme VIII with appropriately adjusted rate constants have been superimposed, demonstrating that Scheme VIII accurately predicts the activation time course in R177Q and R176L channels. As in the fits to wild-type ensemble averages, the early times in the fits to ensemble averages for R176L deviate from the data slightly, likely the result of nonzero prepulse open probabilities that can be corrected in the modeling (data not shown).

In Fig. 18, *C* and *D*, median first latencies for R177Q and R176L channels are plotted as functions of voltage, with median first latencies for wild-type KAT1 superimposed for comparison. The median first latencies for R177Q and R176L are shorter at any given voltage compared with wild-type KAT1. The shorter first latencies are consistent with the depolarizing shift of the steady state G(V) relationships seen in both S4 mutants (Fig. 17). The time course of the ensemble averages and first

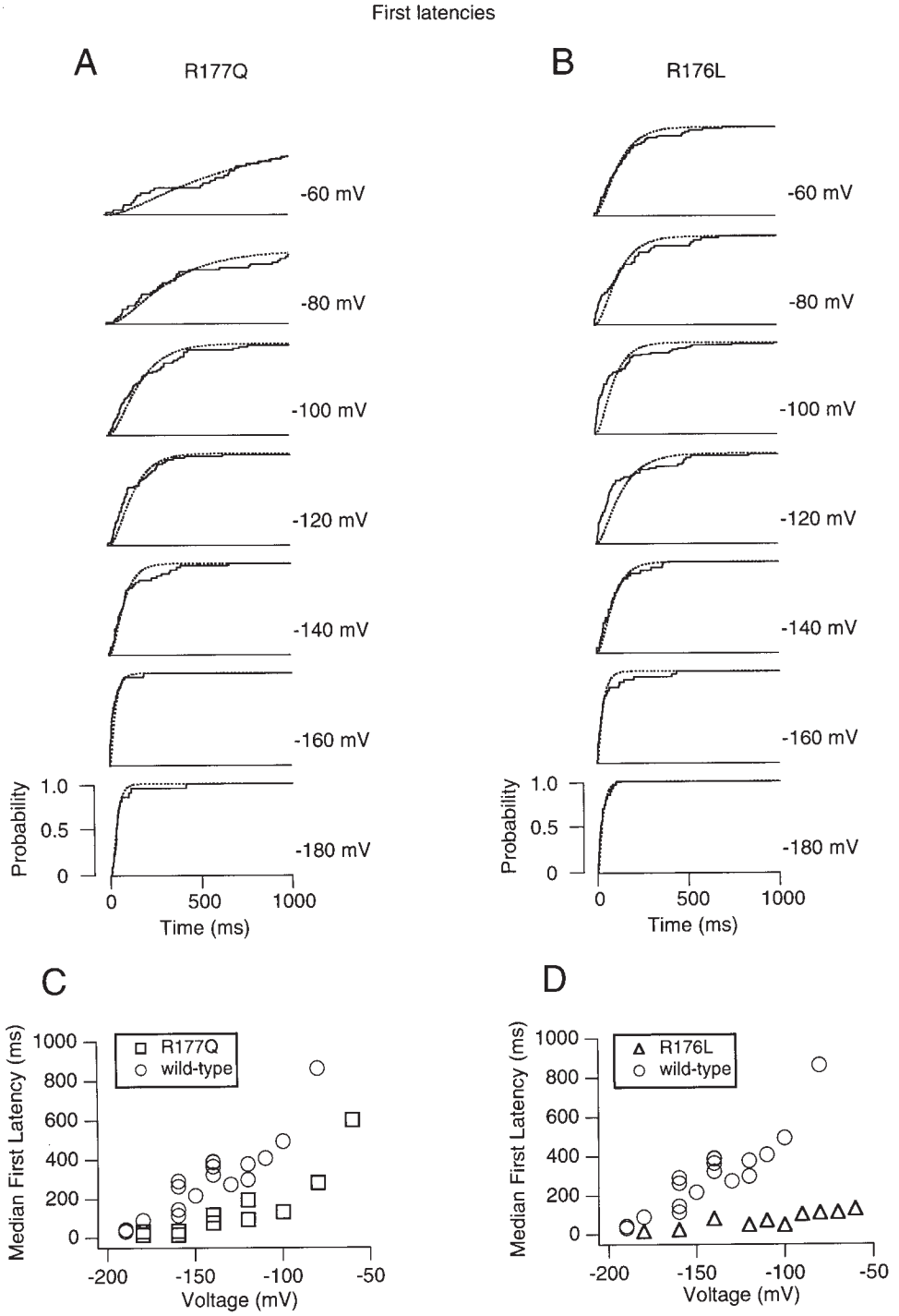

FIGURE 18. (*A*) Cumulative distributions of first latencies recorded at several voltages for R177Q currents. The distributions show the probabilities that the channel first opened by the times indicated. The openings were elicited in response to 1,000–1,600-ms pulses from a prepulse potential of 0 mV. Fits of Scheme VIII to cumulative first latency distributions are superimposed. All rate constants except forward transitions before first opening, k_{01}, k_{12}, and k_{23}, were set to zero over the entire voltage range examined. The solid lines represent the first latency distributions and the dashed lines represent the fits. (*B*) Cumulative distributions of first latencies recorded at several voltages for R176L currents. The conditions are as described in *A*. Fits of Scheme VIII to cumulative first latency distributions are superimposed. (*C*) Median first latencies for R177Q currents (□) are plotted as a function of pulse potential, with median first latencies for wild-type KAT1 superimposed (○). Several patches are represented by the data points. (*D*) Median first latencies for R176L currents (△) are plotted as a function of pulse potential, with median first latencies for wild-type KAT1 superimposed (○). Several patches are represented by the data points.

latency distributions are similar (data not shown), suggesting that, as in wild-type KAT1, transitions leaving the open state do not significantly contribute to KAT1 activation kinetics (Fig. 3 *C*).

Mutations in the S4 Region: Effects on Open States

Fig. 19, *A* and *B*, plot distributions of open times at several voltages for R177Q and R176L channels, respectively, fitted to single exponential functions indicating that R177Q and R176L channels possess only one kinetically discernible open state. Fits to greater than a single exponential did not significantly improve fits. The time constants from the fits to open time distributions are plotted as functions of voltage for R177Q and R176L in Fig. 19, *C* and *D*, with wild-type open times shown for comparison. The open times for R177Q and R176L mutant channels are slightly longer than open

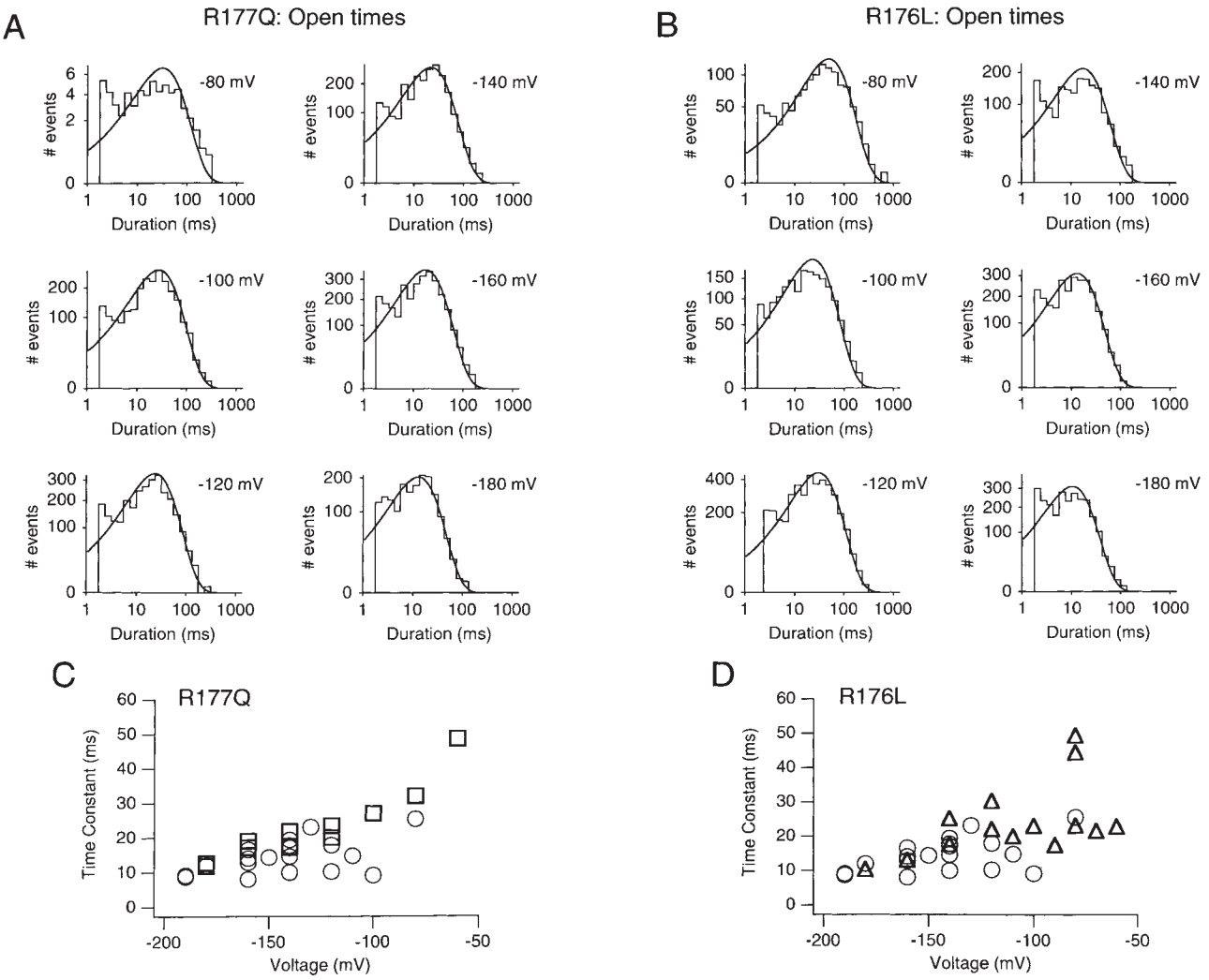

FIGURE 19. (*A*) Frequency histograms of open durations measured at several voltages from R177Q channels, with voltages as indicated. The data were fitted with single exponential functions, represented by the solid curves and displayed as described in METHODS. (*B*) Frequency histograms of open durations measured at several voltages from R176L channels, with voltages as indicated. The data were fitted with single exponential functions, represented by the solid curves and displayed as described in METHODS. (*C*) Voltage dependence of the time constants derived from exponential fits to open time distributions for R177Q currents (□). Open duration time constants for wild-type KAT1 currents are superimposed (○). The data points represent several patches. The open duration distribution time constants have been corrected for missed events as described in METHODS. (*D*) Voltage dependence of the time constants derived from the exponential fits to open time distributions for R176L currents (△). Open duration time constants for wild-type KAT1 currents are superimposed (○). The data points represent several patches.

times in the wild-type channel at any given voltage, suggesting that one or more of the transitions leaving the open state are slower in the mutants than in the wild-type channel. Because the rate constant from the open state into the within-burst closed state (k_{34}) is significantly faster than the rate constant from the open state to the interburst closed state (k_{32}), altering the rate constant k_{32} should have only small effects on the observed open durations. The observed modest effects of the S4 mutations on the open times are consistent with a slowing of k_{32}.

Mutations in the S4 Region: Effects on Closed States After First Opening

The closed-time distributions for R177Q and R176L channels at several voltages are shown in Fig. 20, *A* and *B*, respectively. The data are well fitted by a sum of two exponentials, as additional exponential components did not significantly improve the fits. In Fig. 20, *C* and *D*, the time constants and relative amplitudes of the brief and long components derived from these fits are shown, with corresponding data for the wild-type chan-

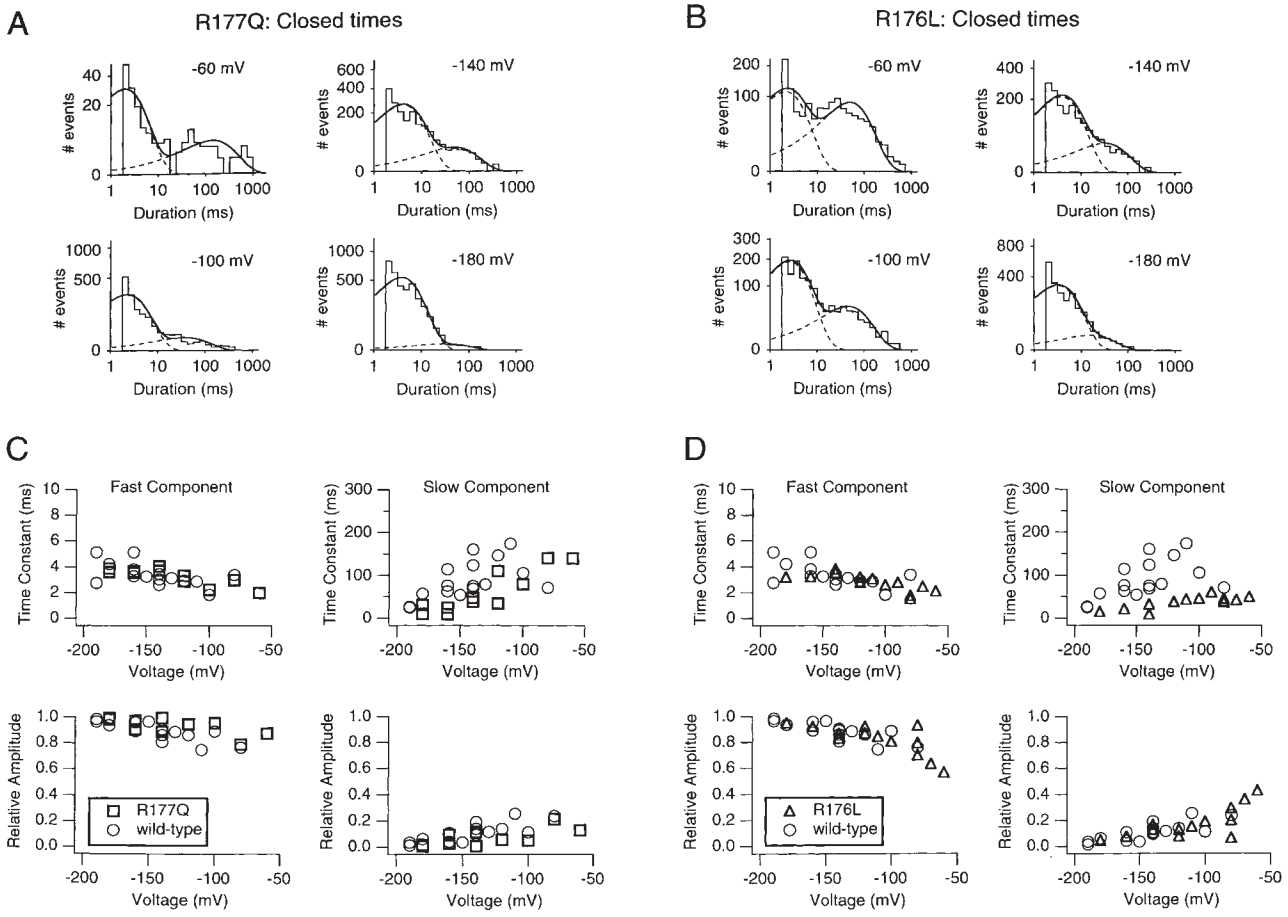

FIGURE 20. (*A*) Frequency histograms of closed durations measured at several voltages for R177Q currents. The data were fitted with a sum of two exponential functions. The solid curves represent the overall fits, and the dashed curves represent the individual exponential components. The data are displayed as described in METHODS. (*B*) Frequency histograms of closed durations measured at several voltages for R176L currents. The data were fitted with a sum of two exponential functions. The solid curves represent the overall fits, and the dashed curves represent the individual exponential components. The data are displayed as described in METHODS. (*C*) Voltage dependence of the time constants and relative amplitudes for the fast and slow exponential components of the fits to R177Q closed-time distributions (□). Corresponding data from wild-type KAT1 currents have been superimposed (○). (*D*) Voltage dependence of the time constants and relative amplitudes for the fast and slow exponential components of the fits to R176L closed-time distributions (△). Corresponding data from wild-type KAT1 currents have been superimposed (○).

nel superimposed for comparison. Neither the R177Q nor R176L mutations significantly alter the relative amplitudes of the long and brief closed-time components. The long component time constant, however, is noticeably shorter in both R177Q and R176L compared with the wild type.

In Fig. 21, *A* and *B*, the time constants derived from single exponential fits to interburst closed-time distributions at several voltages are shown, along with corresponding data from wild-type KAT1 for comparison. As in wild-type KAT1, a burst criterion of 20 ms was used. The time constants from these fits are shorter than those for wild-type KAT1, reflecting shorter sojourns into the interburst closed state in the mutants. The effect of these S4 mutations is consistent with shifting the occupancy of states in the proposed kinetic model towards the right in the kinetic scheme for KAT1 and increasing the rate constants of the transitions leaving the interburst closed state. In Fig. 21, *C* and *D*, the time constants from single exponential fits to within-burst closed-time distributions are shown at several voltages for R177Q and R176L channels, respectively, with data from wild-type KAT1 superimposed for comparison. The within-burst closed-time distributions are unchanged by the S4 substitutions and remain relatively voltage independent over the voltage range examined, indicating that the alterations in the S4 region have little effect on the transition from the within-burst closed state to the open state.

In Fig. 21, *E* and *F*, the probability of terminating a

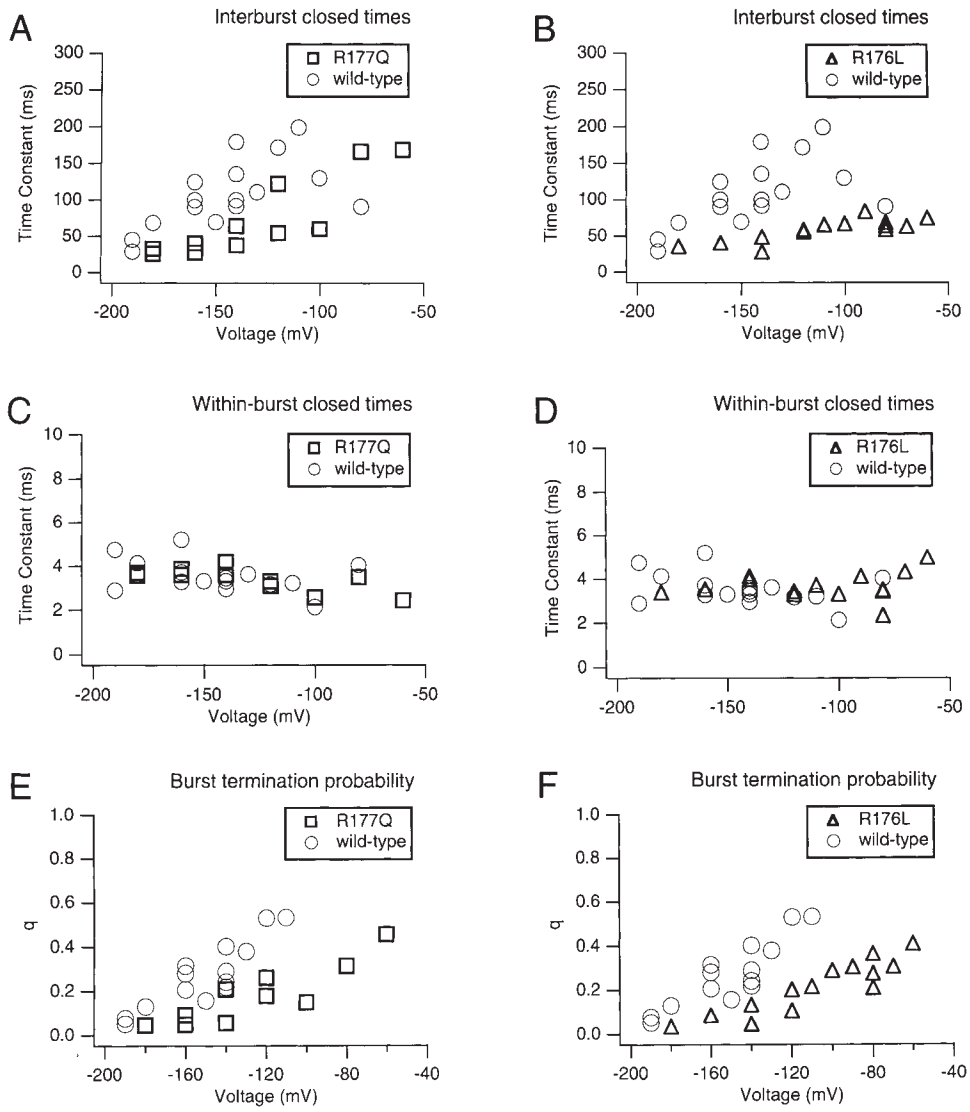

FIGURE 21. (*A* and *B*) Time constants from single exponential fits to interburst closed time distributions for R177Q (□) and R176L (△) currents are plotted as functions of voltage (□). Interburst duration distribution time constants from wild-type KAT1 currents are superimposed (○). (*C* and *D*) The time constants from single exponential fits to the within-burst closed time distributions for R177Q (□) and R176L (△) currents are plotted as functions of voltage. Corresponding time constants from wild-type KAT1 currents are superimposed (○). (*E* and *F*) The probability of terminating a burst (*q*) derived from geometric fits to the distributions of the number of openings per burst is plotted as functions of voltage for R177Q (□) and R176L (△) currents. Corresponding data for wild-type KAT1 currents are superimposed for comparison. A burst criterion of 20 ms was used in all analysis in this figure.

burst (*q*) derived from geometric fits (Eq. 6) to the distribution of the number of openings per burst is plotted as a function of voltage for R177Q and R176L channels, with *q* for wild-type KAT1 channels plotted simultaneously as a function of voltage for comparison. For both mutant channels, the probability of terminating a burst is significantly smaller compared with wild type. Because the within-burst closed-time distributions are unchanged and open-time distributions are only slightly increased, an observed increased burst duration in these mutants can therefore be accounted for primarily by the persistence of these channels in the open and within-burst closed (bursting) states rather than increased dwell times in either of these states. The decrease in burst termination probability in these mutants also accounts in large part for the depolarizing shift in the G(V) relationship in R177Q and R176L channels compared with wild-type channels. Furthermore, comparison of measured burst durations and burst durations calculated from the burst analysis using Eq. 7 for R177Q and R176L channels demonstrates close agreement, which confirms that the proposed bursting model describes the data well (data not shown), as it did for wild-type data.

Mutations in the S4 Region: Effects on the Kinetic Scheme for KAT1 Gating

The rate constants in Scheme VIII are calculated and plotted as functions of voltage for R177Q and R176L channels in Figs. 22 and 23, respectively. The corresponding rate constants calculated for wild-type KAT1 have been superimposed for comparison. The two S4 mutations have no effect on the two transitions located after the open state, k_{34} and k_{43}. Both mutations increased the rate constant from the interburst state to the open state, k_{23}, reflecting the overall faster activation kinetics and shorter sojourns in the interburst

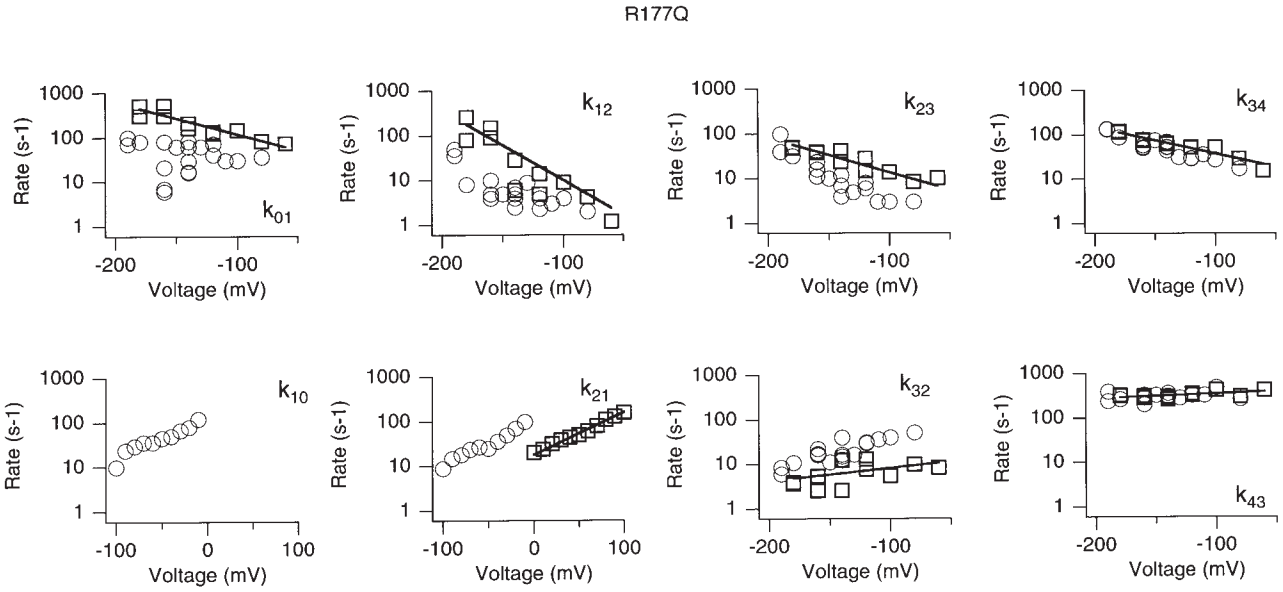

FIGURE 22. Rate constants for Scheme VIII are plotted as a function of voltage for R177Q currents (□). The rate constants k_{23}, k_{34}, k_{32}, and k_{43} were determined by burst analysis as described in the text, while the rate constants k_{01} and k_{12} were determined by fits of the model to the first latency distributions and ensemble averages, given the rate constants determined by burst analysis. The rate constants k_{10} and k_{21} were set to zero over the activation voltage range between −100 and −180 mV. Several patches are represented by the data points. The rate constants k_{10} and k_{21} were determined by fits of Scheme VIII to deactivation tails measured using the cut-open oocyte clamp technique. Tail currents were elicited using an activating pulse to −160 mV. Each rate constant has been fitted to the single exponential function $k_n = n_0 e^{-z_n FV/RT}$, represented by the solid lines, where n_0 is the rate constant at 0 mV, z_n is the equivalent charge, and F, R, and T have their usual meanings. Corresponding rate constants for wild-type KAT1 currents have been superimposed (○).

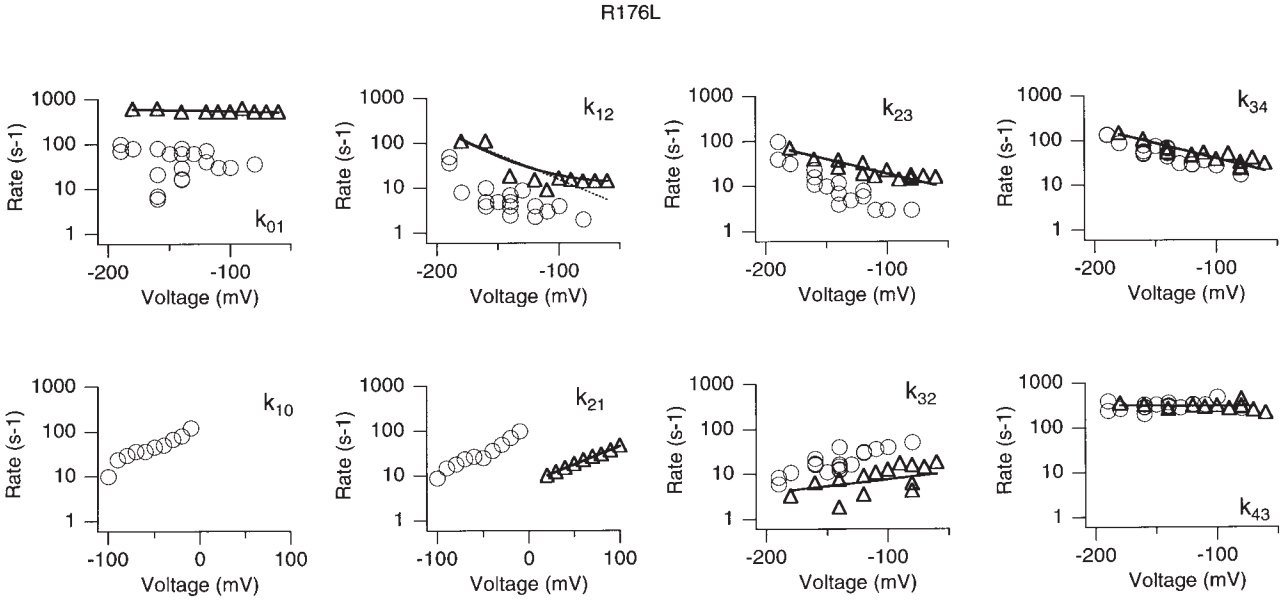

FIGURE 23. Rate constants for Scheme VIII are plotted as a function of voltage for R176L currents (△). The rate constants k_{23}, k_{34}, k_{32}, and k_{43} were determined by burst analysis as described in the text, while the rate constants k_{01} and k_{12} were determined by fits of the model to the first latency distributions and ensemble averages, given the rate constants determined by burst analysis. The rate constants k_{10} and k_{21} were set to zero over the activation voltage range between −100 and −180 mV. Several patches are represented by the data points. The rate constants k_{10} and k_{21} were determined by fits of Scheme VIII to deactivation tails measured using the cut-open oocyte clamp technique. Deactivation tail currents used in these fits were elicited using an activating pulse to −160 mV. Each rate constant except k_{12} has been fitted to the single exponential function $k_n = n_0 e^{-z_n FV/RT}$, represented by the solid lines, where n_0 is the rate constant at 0 mV, z_n is the equivalent charge, and F, R, and T have their usual meanings. The rate constant was fitted to the equation $k_n = a + n_0 e^{-z_n FV/RT}$. Corresponding rate constants for wild-type KAT1 currents have been superimposed (○).

state in the mutant channels compared with the wild type. On the other hand, the reverse transition, k_{32}, from the open state to the interburst closed state, is slower in the R177Q and R176L mutations, reflecting these channels' reluctance to leave the bursting states at hyperpolarized potentials.

In both S4 mutants, very few blank sweeps were observed at all voltages examined, as the cumulative first latencies shown earlier demonstrate (Fig. 18). The cumulative first latency distributions reach a steady state value of one at most voltages examined. Therefore, the contribution of both right censor error as well as the inactivated state is reduced in the mutants. In fact, the inclusion of the inactivated state was not necessary to account for the first latency distributions and ensemble averages for the mutants in order to adequately fit Scheme VIII to the data.

Individual fits of Scheme VIII to ensemble averages and first latencies for R177Q and R176L channels were shown earlier in Figs. 17 and 18. As in wild-type KAT1 channels, the reverse transitions k_{10} and k_{21} were set to zero in deriving these fits. Both R177Q and R176L mutations increase rate constants k_{01} and k_{12} compared with wild-type KAT1, reflecting the faster time courses of activation and shorter first latency distributions for both mutant channels. As demonstrated earlier for wild-type KAT1, a model that incorporates the proposed tetrameric quaternary structure of KAT1 using a Hodgkin-Huxley assumption of independent and identical subunits predicts too much sigmoidal delay in the activation time course.

The reverse transitions k_{10} and k_{21} were determined in the depolarized voltage range more positive than 0 mV by fitting Scheme VIII to deactivation tail currents obtained from R177Q and R176L channels (data not shown). In fitting the deactivation tails, the kinetics were found to be largely determined by the reverse transition k_{32} and to a smaller extent by the reverse transition k_{21}. The earlier transitions (k_{01}, k_{10}, and k_{12}) contribute little to the tail kinetics, and therefore are not as well determined in this way. This is because, in the depolarized voltage range, the forward transitions k_{01}, k_{12}, and k_{23} are extraordinarily small, so that once the channel closes to C_2 it is unlikely to reopen. This feature of the model could be tested by observing the number of reopening events in single channel deactivation tails in the depolarized voltage range; however, these measurements are experimentally difficult given the small current in that voltage range due to a decreased driving force, as well as pore-determined rectification. Note also that values for the rate constant k_{32} were determined by burst analysis in the hyperpolarized voltage range, extrapolated, and allowed to relax in fits to the deactivation tail currents.

The deactivation tail currents predicted by the model are somewhat faster than the observed deactivation tail currents specifically for R176L. This could be explained if one or more of the rate constants in the model do not follow a strictly single exponential voltage dependence. These slower tail currents could be accounted for if (*a*) the reverse transition k_{32} were slower than predicted, or (*b*) if the forward transition k_{34} were faster than predicted by the model. The effect of both of these alterations in the model is to decrease the probability of terminating a burst and could be differentiated by examining single channel currents using burst analysis in the extremely depolarized voltage range. However, again because of the KAT1 channel's

TABLE III

Summary of the Fits to the Rate Constants for Scheme VIII for R177Q and R176L Channels

	R177Q		R176L		Wild type	
Rate	n_0 (s^{-1})	z_n (e^- charges)	n_0 (s^{-1})	z_n (e^- charges)	n_0 (s^{-1})	z_n (e^- charges)
k_{01}	21.5	0.42	456	0.034	11.8	0.24
k_{12}	0.274	0.91	(12.0) 0.228	0.87	1.17	0.26
k_{23}	2.51	0.42	4.35	0.38	0.24	0.71
k_{34}	9.55	0.35	8.53	0.39	3.67	0.47
k_{10}	—	—	—	—	139	−0.57
k_{21}	18.0	−0.55	6.98	−0.47	126	−0.71
k_{32}	15.7	−0.17	15.6	−0.18	186	−0.40
k_{43}	454	−0.062	301	0.00	430	−0.056

Amplitude and equivalent charge derived from exponential fits to the rate constants in Scheme VIII for wild-type, R177Q, and R176L channels. Each rate constant has been fitted with a single exponential function: $k_n = n_0 e^{-z_n FV/RT}$, where V is voltage and *F*, *R*, and *T* have their usual meanings. The exponential fit for the rate constant k_{12} required the introduction of a constant offset factor for a good fit, and was therefore fitted with the equation: $k_n = a + n_0 e^{-z_n FV/RT}$, where *a* is the offset factor indicated in the parenthesis. The absolute values of the total charges derived from summing the individual rate constants are at least 2.88e for R177Q and 2.32e for R176L. The absolute values of the apparent charges derived from Boltzmann fits, in comparison are 1.37e for R177Q and 0.54e for R176L. In general, the rate constants closer to the open state are more important in determining the quantitative fits to the data, and are therefore better determined than the other rate constants.

pore-determined inward rectification properties, outward single channel currents in this voltage range would be difficult to measure.

The voltage dependences of the rate constants from Scheme VIII in Figs. 22 and 23 have been fitted to single exponential functions using Eq. 8. The amplitudes and equivalent charges derived from these fits are shown in Table III for each individual rate constant, with corresponding data for wild-type KAT1 included for comparison. Note that for the R176L channel, the voltage dependence of the rate constant k_{12} requires fitting to a single exponential function that includes a linear offset. This modification was introduced because, at less negative potentials, the value of this rate constant failed to continue to decline in a single exponential fashion. The existence of a linear offset may imply that either the rate constant represents an amalgamation of several transitions, or that the conformational change represented by this rate constant possesses a voltage-independent component. A nonexponential voltage dependence may imply that the dipole associated with that particular voltage-dependent transition is itself dependent on voltage (Stevens, 1978). Interestingly, this linear offset was not required for fits to the same rate constant in R177Q and wild-type channels.

The measured steady state G(V) for R177Q and R176L currents are well fitted by the model (Fig. 24). The magnitudes of the total charges derived by adding all the individual equivalent charges for each rate constant in Scheme VIII are at least 2.88 and 2.32e for R177Q and R176L, respectively (compared with 3.42e for the wild-type channel). These values are underestimates, as the first backward rate constant, k_{10}, was not well determined in the mutants. In contrast, the magnitudes of the apparent gating charges derived from fits of the G(V)s for both mutants to Boltzmann functions are 1.37e for R177Q and 0.54e for R176L (compared with 1.36e for the wild type), again highlighting the unclear nature of estimating total gating charge from fits of the data by Boltzmann functions.

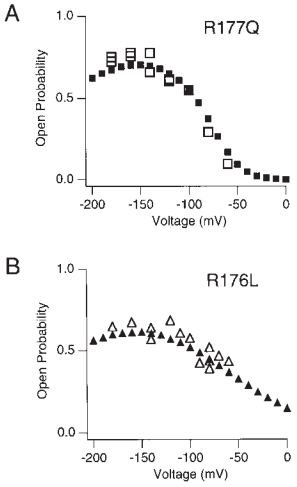

FIGURE 24. (*A*) Fits of Scheme VIII to the single channel g(V) relationship for R177Q currents. □ represent measured steady state open probabilities, while ■ represent fits from the model. The fits derived from the model were determined by measuring steady-state open probabilities from calculated open probability waveforms over the voltage range shown. (*B*) Fits of Scheme VIII to the single channel G(V) relationship for R176L currents. △ represent measured steady state open probabilities, while ▲ represent fits from the model. The open probabilities derived from the model were determined by measuring steady state open probabilities from calculated open probability waveforms over the voltage range shown.

Using the rate constants derived in Figs. 22 and 23, the free energy differences between each of the individual contiguous states in Scheme VIII can be calculated with the following equation:

$$\Delta G = RT\ln\left(\frac{k_f}{k_r}\right), \tag{9}$$

where R is the universal gas constant, T is absolute temperature, k_f is the rate constant of the forward transition, and k_r is the rate constant of the reverse transition. The free energy difference reflects the relative stability of each channel conformation represented in the model. Furthermore, the activation energy reflected by the transition rate constants away from each conformational state of the channel can be estimated by the following equation:

$$\Delta G^{++} = -RT\ln\left(\frac{k}{\upsilon}\right), \tag{10}$$

where k is the transition rate and υ is the product of the transmission coefficient and the molecular vibration frequency and is assumed to have a value of 10^{12} s^{-1}. The estimated energy barriers all lie within the range between 12 and 18 kcal · mol^{-1}, well above the thermal energy (0.6 kcal · mol^{-1}). The molecular vibration frequency can be as low as 10^9 s^{-1}. If this lower vibration frequency is used, the activation energies will be decreased in magnitude by ~78%. However, the overall observed trends will not be altered.

The value for the rate constant k_{10}, and hence activation energy from state C_1 to state C_0, was not well determined by the data for R177Q and R176L channels. Therefore, the relative energy difference between states C_0 and C_1 can only be estimated. From calculations of all activation energies and relative energies between states in the model for mutant and wild-type KAT1 channels over the voltage range examined, several observations can be made. Activation energies and conformational state energies after the open state are not altered by the S4 mutations, while all transitions and state energies before the open state are altered. The S4 mutations increase the relative energies of the closed states before first opening, with the changes introduced by R176L greater than those of R177Q. The effects of the R177Q and R176L mutations on the conformational states and transitions in Scheme VIII summarized in this way indicate that only the transitions and states before the open state are significantly altered. This result suggests that the transitions between conformational states before the open state involve the

S4 region, while transitions after the open state most likely do not. This is consistent with results seen with mutations in the S4 region of other voltage-gated channels, suggesting a common structural mechanism in voltage-dependent gating, despite the fact that KAT1 is an inward rectifier, while the other channels studied are outward rectifiers.

DISCUSSION

Several conclusions can be made about the KAT1 channel that are independent of the specific assumptions and models used in this article. (*a*) The single channel conductance in symmetrical K^+ solutions is ~7.5 pS, and the open channel permeation properties demonstrate inward rectification only at positive voltages in symmetrical K^+ solutions, accounting for only a small part of the channel's inward rectification properties. This is in contrast with the small inward rectifiers, in which inward rectification results from pore block by Mg^{2+} and polyamines (Kubo et al., 1993*a,b*; Ficker et al., 1994; Lopatin et al., 1994; Nichols et al., 1994; Fakler et al., 1995). (*b*) The activation time course is slow and voltage dependent, on the order of several hundred milliseconds. Moreover, deactivation is relatively fast and becomes faster with more positive voltages, with a time scale on the order of tens of milliseconds. (*c*) Transitions before first opening account for a large portion of the voltage dependence of KAT1 activation, as seen in *Shaker*-family channels (Zagotta and Aldrich, 1990; Hoshi et al., 1994; Zagotta et al., 1994*a,b*; Schoppa and Sigworth, 1998*a,c*). (*d*) Multiple closed states are traversed from the resting to the open channel via voltage-dependent transitions, as demonstrated in *Shaker*-family channels (Zagotta and Aldrich, 1990; Hoshi et al., 1994). (*e*) There is only one kinetically discernible open state in KAT1 gating with exit rates that are only slightly voltage dependent. (*f*) The KAT1 channel displays no appreciable time-dependent inactivation process. However, the existence of blank sweeps not accounted for by the right censor time necessitates the inclusion of an inactivated state accessible from early closed states. This inactivated state is more pronounced at depolarized potentials. (*g*) The transition to closed states after first opening are only slightly voltage dependent. In *Shaker*-family channels, a similar relatively short lived, as well as an intermediate lived, voltage-independent closed state located after the open state has been described (Hoshi et al., 1994). (*h*) The general gating characteristics of cloned KAT1 channels are similar to channels recorded from native tissue (Schroeder and Fang, 1991; Sussman et al., 1994).

Several kinetic models were considered to account for the gating behavior of KAT1 channels. Among the two possible bursting schemes, the COC configuration was considered to be the superior scheme to account for the bursting behavior of KAT1 in the context of the overall voltage dependence of KAT1 channel activation. The single channel and macroscopic data are best described by Scheme VIII. The overall voltage dependence of KAT1 gating is distributed approximately equally over the transitions before the open state, rather than being isolated to a single transition or a subset of transitions, similar to kinetic schemes described for *Shaker*-family channels (Zagotta et al., 1994*b*; Schoppa and Sigworth, 1998*c*).

There are several limitations to the final proposed kinetic model for KAT1 depicted in Scheme VIII. (*a*) The slow creep seen in some of the first latency distributions suggests that there may be a closed state that branches from one of the closed states along the inactivation pathway. (*b*) The occasional observation of current rundown has not been incorporated into the model. However, rundown occurred infrequently, so that it was reasonable to not incorporate it into the final kinetic scheme. (*c*) Not all rate constants in the model are equally well determined. For Scheme VIII, the rate constants k_{23}, k_{34}, k_{32}, and k_{43} are well determined by the burst analysis, with k_{34}, k_{32}, and k_{43} overdetermined by multiple bursting parameters. k_{01} and k_{12} were determined by first latency and ensemble average data. k_{10} and k_{21} were assumed to be zero at hyperpolarized potentials and were determined by fits of the model to macroscopic tail currents at depolarized potentials. Therefore, the values of these reverse transitions are not as well determined as the values of the other transitions in the model. (*d*) It has been assumed in many kinetic models of voltage-dependent gating of various channels that the voltage dependence of transitions between kinetically distinguishable states is exponentially determined. However, it has been suggested that voltage-dependent transitions do not necessarily behave in this fashion (Stevens, 1978). The kinetic model used to describe KAT1 produces rate constants that display single exponential voltage dependence. This result implies that perhaps the rate constants described by the model represent individual voltage-dependent conformational changes, rather than a composite of a series of conformational changes. (*e*) The voltage range for single channel current recordings was limited by experimental conditions. Voltages more negative than −190 mV were not examined because the long pulse durations at extremely negative voltages were not well tolerated by membrane patches. Given the symmetrical K^+ solutions, voltages more positive than approximately −100 to −80 mV resulted in currents that were too small to resolve, given the low open probability and small unitary conductance of KAT1 at depolarized voltages.

In wild-type KAT1 and in both S4 mutants, the total

gating charge derived by adding the individual gating charges associated with each rate constant in the model was substantially larger than the apparent charge obtained from fitting the G(V) relationships to Boltzmann functions. This discrepancy highlights the caution warranted in interpreting parameters obtained from Boltzmann fits. The gating model developed for KAT1 is significantly different from the simple two-state (open and closed) model assumed when applying a Boltzmann fit to the G(V) relationship. A discrepancy between total charge measured by various means and apparent charge derived from fits to Boltzmann functions has been demonstrated previously in *Shaker*-family channels (Zagotta et al., 1994*b*; Schoppa and Sigworth, 1998*c*).

The kinetic model described in Scheme VIII implies the existence of at least three individual transitions before first opening that appear to require concerted movements of the presumed KAT1 tetramer, and there is no evidence for fourfold symmetry in the gating transitions, as seen in *Shaker*-like channels (Zagotta and Aldrich, 1990; Hoshi et al., 1994; Zagotta et al., 1994*a,b*; Schoppa and Sigworth, 1998*a,b,c*). This result is not necessarily counter to the proposed fourfold symmetry of the KAT1 structure. There is evidence of concerted gating processes in other channels that possess multiple-subunit structural symmetry. *Shaker* channels appear to undergo one or more concerted transitions during the last step in activation before channel opening (Hoshi et al., 1994; Zagotta et al., 1994*a,b*; Schoppa and Sigworth, 1998*a,b,c*; Smith-Maxwell et al., 1998). *Shaker* channels undergo at least two types of inactivation processes, N-type (Hoshi et al., 1990; Zagotta et al., 1990) and C-type (Hoshi et al., 1991) inactivation, that do not involve obligate independent and identical subunit transitions. In the small inward rectifiers, single channel data imply that in addition to the independent transitions that gate the individual subunits of the triple-barrel structure, a concerted transition also occurs to gate the entire triple barrel channel (Matsuda, 1991). Alternatively, Scheme VIII may represent a model that incorporates fourfold structural symmetry if the early transitions involving conformational changes in the individual subunits are not observable because the overall equilibrium favors partially activated states. Then, the states and transitions represented by Scheme VIII would be equivalent to the final concerted transition(s) described for *Shaker* channels (Zagotta et al., 1994*b*; Schoppa and Sigworth, 1998*c*).

The effects of two mutations in the S4 region of the KAT1 channel, R177Q and R176L, on single channel gating properties were examined. These mutations change charged arginine (R) residues to either a glutamine (Q) or a leucine (L). Several conclusions about the effects of these mutations on the gating properties of KAT1 can be made that are independent of any kinetic model proposed. (*a*) These mutations have minimal effects on the open channel conductance, consistent with the presumption that the S4 region does not contribute to the pore-forming regions of the KAT1 channel. (*b*) Both S4 mutations shifted the steady state open probability voltage dependence relationships in the positive direction, with the R176L mutation resulting in a greater depolarizing shift. The R176L mutation decreased the apparent charge derived from a Boltzmann fit to the steady state G(V) relationship, while the R177Q mutation did not alter the apparent charge. (*c*) In both mutations, the first latency distributions and the kinetics of the ensemble averages were faster than that in wild type for a given voltage. (*d*) The mutations did not alter closed times within bursts, while interburst durations are shorter in the two S4 mutants compared with wild-type KAT1. (*e*) The probability of terminating a burst (q) is smaller in the S4 mutants compared with wild-type KAT1, and q becomes smaller with increasing hyperpolarization over the voltage range examined. (*f*) There are significantly fewer blank sweeps in both S4 mutants compared with wild-type KAT1.

The minimal kinetic scheme presented can adequately describe the voltage-dependent gating behavior of the R177Q and R176L mutant channels by merely altering the values of the individual rate constants without changing the overall connectivity between conformational states in the model. Burst analysis revealed that transitions into and away from the within-burst closed state are brief and unaffected by the S4 mutations, while the transitions into and away from the interburst closed state are altered by the S4 mutations. The transition from the interburst closed state to the open state is faster at all voltages examined, while the reverse transition from the open state to the interburst closed state is slower at all voltages examined in the two mutants compared with wild-type KAT1. Overall, the S4 mutations increased all forward transition rates along the activation pathway while decreasing all backward transition rates before the open state. Moreover, the total charge derived from summation of the individual charges for rate constants in the model were altered modestly by the two S4 mutants, even R176L, in contrast to the large change in apparent charge derived from Boltzmann fits.

These results suggest several implications about the structural determinants of KAT1 voltage-dependent gating. The S4 mutations destabilize all closed states before the open state, favoring rightward-located states in the model. In *Shaker*-family channels, most mutations introduced in the S4 region also result in rightward shifts in the G(V) relationships, even though rightward G(V) shifts in *Shaker* favor closed states over open, while in KAT1 open states are favored over closed. This

suggests that the equilibrium between possible physical conformations of the S4 region is affected in the same way by S4 mutations in both classes of channels. Perhaps then the fundamental response of the S4 region to voltage is similar in KAT1 and *Shaker*-family channels, but the coupling of S4 movement to channel opening has opposite polarity in these two channel proteins. For instance, the S6 region of the pore structure appears to act as a gate (Liu et al., 1997) that may be coupled to the S4 region with opposite polarity in KAT1 and *Shaker*-family channels.

Furthermore, these results suggest that the transitions located along the activation pathway are likely to involve conformational changes in the S4 region of KAT1, a conclusion also drawn for *Shaker*-family channels (Timpe et al., 1988; Stühmer et al., 1989; Liman et al., 1991; Papazian et al., 1991; Logothetis et al., 1992; Schoppa et al., 1992; Tytgat and Hess, 1992; Logothetis et al., 1993; Shao and Papazian, 1993). As the S4 mutations have no effect on transitions after the open state, it is reasonable to conclude that the transitions between the open and within-burst closed states probably do not involve conformational changes in the S4 region. Perhaps the S4 region in KAT1 is involved in the voltage-dependent activation process up to channel opening, while transitions after the open state involve a different structural mechanism. This alternative mechanism, which results in the observed bursting phenomenon in KAT1, might result from brief closures involving the pore forming regions of the channel, or perhaps a fast blocking process.

The KAT1 channel straddles the division between outward rectifiers such as the *Shaker*-family channels and the small inward rectifiers such as IRK, GIRK, and ROMK. The KAT1 channel structurally resembles other *Shaker*-family channels, yet it behaves as an inward rectifier. The herg channel is also structurally similar to *Shaker*-family channels, and it also demonstrates inward rectification properties under specific conditions. However, the herg channel also has properties of outward rectification under physiological conditions (Curran et al., 1995; Trudeau et al., 1995). Mutagenesis analysis in herg suggests that a C-type inactivation process may play a role in the inward rectification seen in herg, as mutations in the pore region and external K^+ affect herg currents (Schonherr and Heinemann, 1996; Smith et al., 1996). Moreover, mutagenesis in the *Shaker* channel has demonstrated that inwardly rectifying channels can be created from outwardly rectifying *Shaker*-like channels by altering the voltage-dependent kinetic properties of NH_2-terminal inactivation (Miller and Aldrich, 1996). The gating mechanism of KAT1 therefore appears to be dissimilar to that of herg, as the analysis in this article, taken together with other work (Hoshi, 1995; Marten and Hoshi, 1997), demonstrates that the KAT1 channel does not use an inactivation recovery mechanism in gating.

BCNG, a channel responsible for pacemaker activity in brain and possibly the heart is similar to KAT1 in that it possesses six transmembrane regions, a *P* region, and an S4 region (Santoro et al., 1998). The gating properties of BCNG are remarkably similar to that of KAT1, including inward rectification, slow, sigmoidal activation, an extremely negative range of activation (more negative than −80mV), and relatively fast deactivation tail currents that demonstrate a rising phase. Given the striking similarities in gating kinetics, perhaps KAT1 and BCNG share a similar gating mechanism that involves the S4 region rather than recovery from inactivation. This possibility can be evaluated in the BCNG channel through mutagenesis at residues in the NH_2 and COOH termini that are possibly involved in inactivation, and at residues in the S4 region as examined in this article for KAT1.

The data presented in this article suggest that a novel gating mechanism unlike that seen in other inward rectifiers results in the inward rectification properties of KAT1. The presence of an S4 region that contains charged residues at every third position suggests that, as in other voltage-gated channels, KAT1 gating may involve the S4 segment. This hypothesis implies that the inward rectifying phenotype of KAT1 results from the channel's intrinsic ability to sense changes in the membrane electric field. However, instead of opening with depolarization, KAT1 channels open with hyperpolarization. The single channel KAT1 currents examined in this article have provided some insight into the gating mechanisms of wild-type and mutant KAT1 channels that should serve as a useful basis for work on the gating mechanism of this interesting channel.

We thank Toshinori Hoshi and Dorothy Perkins for developing software used in the single channel analysis and modeling, Richard F. Gaber for providing us with the KAT1 clone, and Alan Miller for help with the initial molecular biology. We also thank George Martin for technical support.

P.C. Zei was supported by an National Institute of General Medical Sciences Training Grant (GM07365) for the Medical Scientist Training Program. R.W. Aldrich is an investigator with the Howard Hughes Medical Institute.

Original version received 10 June 1998 and accepted version received 1 October 1998.

REFERENCES

Adelman, J.P., K.Z. Shen, M.P. Kavanaugh, R.A. Warren, Y.N. Wu, A. Lagrutta, C.T. Bond, and R.A. North. 1992. Calcium-activated potassium channels expressed from cloned complementary DNA's. *Neuron.* 9:209–216.

Adrian, R.H. 1969. Rectification in muscle membrane. *Prog. Biophys. Mol. Biol.* 19:340–369.

Aggarwal, S.K., and R. MacKinnon. 1994. Contribution of the S4 segment to gating charge in the *Shaker* K^+ channel. *Neuron.* 16: 1169–1177.

Anderson, J.A., S.S. Huprikar, L.V. Kochian, W.J. Lucas, and R.F. Gaber. 1992. Functional expression of a probable *Arabidopsis thaliana* potassium channel in *Saccharomyces cerevisae. Proc. Natl. Acad. Sci. USA.* 89:3736–3740.

Ashford, M.L.J., C.T. Bond, T.A. Blair, and J.P. Adelman. 1994. Cloning and functional expression of a rat heart KATP channel. *Nature.* 370:456–459.

Atkinson, N.S., G.A. Robertson, and B. Ganetzky. 1991. A component of calcium-activated potassium channels encoded by the *Drosophila* slo locus. *Science.* 253:551–555.

Blatz, A.L., and K.L. Magleby. 1986. Correcting single channel data for missed events. *Biophys. J.* 49:967–980.

Butler, A., S. Tsunoda, D.P. McCobb, A. Wei, and L. Salkoff. 1993. mSlo, a complex mouse gene encoding "maxi" calcium-activated potassium channels. *Science.* 261:221–224.

Cha, A., and F. Bezanilla. 1997. Characterizing voltage-dependent conformational changes in the *Shaker* K^+ channel with fluorescence. *Neuron.* 19:1127–1140.

Colquhoun, D., and A.G. Hawkes. 1982. On the stochastic properties of bursts of single ion channel openings and of clusters of bursts. *Philos. Trans. R. Soc. Lond. B Biol. Sci.* 300:1–59.

Colquhoun, D., and A.G. Hawkes. 1995. The principles of the stochastic interpretation of ion-channel mechanisms. *In* Single Channel Recording. Plenum Publishing Corp., New York. 397–482.

Cox, D.H., J. Cui, and R.W. Aldrich. 1997. Separation of gating properties from permeation and block in *mslo* large conductance Ca-activated K^+ channels. *J. Gen. Physiol.* 109:633–646.

Cui, J., D.H. Cox, and R.W. Aldrich. 1997. Intrinsic voltage dependence and Ca^{2+} regulation of mslo large conductance Ca-activated K^+ channels. *J. Gen. Physiol.* 109:647–673.

Curran, M.E., I. Splawski, K.W. Timothy, G.M. Vincent, E.D. Green, and M.T. Keating. 1995. A molecular basis for cardiac arrhythmia: *herg* mutations cause long QT syndrome. *Cell.* 80:795–803.

Dascal, N., N.F. Lim, W. Schreibmayer, W. Wang, N. Davidson, and H.A. Lester. 1993. Expression of an atrial G-protein-activated potassium channel in *Xenopus* oocytes. *Proc. Natl. Acad. Sci. USA.* 90:6596–6600.

Demo, S.D., and G. Yellen. 1991. The inactivation gate of the *Shaker* K^+ channel behaves like an open-channel blocker. *Neuron.* 7:743–753.

Doyle, D.A., J.M. Cabral, R.A. Pfuetzner, A. Kuo, J.M. Gulbis, S.L. Cohen, B.T. Chait, and R. MacKinnon. 1998. The structure of the potassium channel: molecular basis of K^+ conduction and selectivity. *Science.* 280:69–77.

Fakler, B., U. Brandle, E. Glowatski, S. Weidemann, H.-P. Zenner, and J.P. Ruppersberg. 1995. Strong voltage-dependent inward rectification of inward rectifier K^+ channels is caused by intracellular spermine. *Cell.* 80:149–154.

Ficker, E., M. Taglialatela, B.A. Wible, C.M. Henley, and A.M. Brown. 1994. Spermine and spermidine as gating molecules for inward rectifier K^+ channels. *Science.* 266:1068–1072.

Gautam, M., and M.A. Tanouye. 1990. Alteration of potassium channel gating: molecular analysis of the *Drosophila* Sh5 mutation. *Neuron.* 5:67–73.

Hagiwara, S., and K. Takahashi. 1974. The anomalous rectification and cation selectivity of the membrane of a starfish egg cell. *J. Membr. Biol.* 18:61–80.

Hamill, O.P., A. Marty, E. Neher, B. Sakmann, and F.J. Sigworth. 1981. Improved patch-clamp techniques for high-resolution current recording from cells and cell-free membrane patches. *Pflügers Arch.* 391:85–100.

Heginbotham, L., and R. MacKinnon. 1992. The aromatic binding site for tetraethylammonium ion on potassium channels. *Neuron.* 8:483–491.

Hille, B. 1992. Ionic channels of excitable membranes. Sinauer Associates, Inc., Sunderland, MA. 607 pp.

Hille, B., and W. Schwarz. 1978. Potassium channels as multi-ion single-file pores. *J. Gen. Physiol.* 72:409–442.

Ho, K., C.G. Nichols, W.J. Lederer, J. Lytton, P.M. Vassilev, M.V. Kanazirska, and S.C. Hebert. 1993. Cloning and expression of an inwardly rectifying ATP-regulated potassium channel. *Nature.* 362:31–38.

Hodgkin, A.L., and A.F. Huxley. 1952. A quantitative description of membrane curent and its application to conduction and excitation in nerve. *J. Physiol. (Lond.).* 117:500–544.

Horn, R., C.A. Vandenberg, and K. Lange. 1984. Statistical analysis of single sodium channels. Effects of *N*-bromoacetamide. *Biophys. J.* 45:323–335.

Hoshi, T. 1995. Regulation of voltage dependence of the KAT1 channel by intracellular factors. *J. Gen. Physiol.* 105:309–328.

Hoshi, T., and R.W. Aldrich. 1988. Gating kinetics of four classes of voltage-dependent K^+ channels in pheochromocytoma cells. *J. Gen. Physiol.* 91:107–131.

Hoshi, T., and W.N. Zagotta. 1993. Recent advances in the understanding of potassium channel function. *Curr. Opin. Neurobiol.* 3: 283–290.

Hoshi, T., W.N. Zagotta, and R.W. Aldrich. 1990. Biophysical and molecular mechanisms of *Shaker* potassium channel inactivation. *Science.* 250:533–538.

Hoshi, T., W.N. Zagotta, and R.W. Aldrich. 1991. Two types of inactivation in *Shaker* K channels: effects of alterations in the carboxy-terminal region. *Neuron.* 7:547–556.

Hoshi, T., W.N. Zagotta, and R.W. Aldrich. 1994. *Shaker* potassium channel gating I: transitions near the open state. *J. Gen. Physiol.* 103:249–278.

Inagaki, N., T. Gonoi, J.P. Clement IV, N. Namba, J. Inazawa, G. Gonzalez, L. Aguilar-Bryan, S. Seino, and J. Bryan. 1995. Reconstitution of I_{KATP}: an inward rectifier subunit plus the sulfonylurea receptor. *Science.* 270:1166–1170.

Jackson, M.B., B.S. Wong, C.E. Morris, H. Lecar, and C.N. Christian. 1983. Successive openings of the same acetylcholine receptor are correlated in open time. *Biophys. J.* 42:109–114.

Kamb, A., L.E. Iverson, and M.A. Tanouye. 1987. Molecular characterization of *Shaker*, a *Drosophila* gene that encodes a potassium channel. *Cell.* 50:405–413.

Katz, B. 1949. Les constantes electriques de la membrane du muscle. *Arch. Sci. Physiol.* 2:285–299.

Krapivinsky, G., E.A. Gordon, K. Wickman, B. Velimirovic, L. Krapivinsky, and D.E. Clapham. 1995. The G-protein-gated atrial K^+ channel IKACh is a heteromultimer of two inwardly rectifying K^+ channel proteins. *Nature.* 374:135–141.

Kubo, Y., T.J. Baldwin, Y.N. Jan, and L.Y. Jan. 1993*a*. Primary structure and functional expression of a mouse inward rectifier potassium channel. *Nature.* 362:127–133.

Kubo, Y., E. Reuveny, P.A. Slesinger, Y.N. Jan, and L.Y. Jan. 1993*b*. Primary structure and functional expression of a rat G-protein-coupled muscarinic potassium channel. *Nature.* 364:802–806.

Larsson, H.P., O.S. Baker, D.S. Dhillon, and E.Y. Isacoff. 1996.

Transmembrane movement of the *Shaker* K^+ channel S4. *Neuron.* 16:387–397.

Lawless, J.F. 1982. Statistical models and methods for lifetime data. John Wiley & Sons, Inc., New York. 580 pp.

Lichtinghagen, R., M. Stocker, R. Wittka, G. Boheim, W. Stuhmer, A. Ferrus, and O. Pongs. 1990. Molecular basis of altered excitability in *Shaker* mutants of *Drosophila melanogaster. EMBO (Eur. Mol. Biol. Organ.) J.* 9:4399–4407.

Liman, E.R., P. Hess, F. Weaver, and G. Koren. 1991. Voltage-sensing residues in the S4 region of a mammalian K^+ channel. *Nature.* 353:752–756.

Liu, Y., M. Holmgren, M.E. Jurman, and G. Yellen. 1997. Gated access to the pore of a voltage-dependent K^+ channel. *Neuron.* 19:175–184.

Logothetis, D.E., B.F. Kammen, K. Lindpaintner, D. Bisbas, and B. Nadal-Ginard. 1993. Incremental reductions of positive charge within the S4 region of a voltage-gated K^+ channel result in corresponding decreases in gating charge. *Neuron.* 8:531–540.

Logothetis, D.E., S. Mohavedi, C. Satler, K. Lindpaintner, and B. Nadal-Ginard. 1992. Gating charge differences between two voltage-gated K^+ channels are due to the specific charge content of their respective S4 regions. *Neuron.* 10:1121–1129.

Lopatin, A.N., E.N. Makhina, and C.G. Nichols. 1994. Potassium channel block by cytoplasmic polyamines as the mechanism of intrinsic rectification. *Nature.* 372:366–369.

Lopez-Barneo, J., T. Hoshi, S.H. Heinemann, and R.W. Aldrich. 1992. Effects of external cations and mutations in the pore region on C-type inactivation of *Shaker* potassium channels. *Receptors Channels.* 1:61–71.

MacKinnon, R. 1991. Determination of subunit stoichiometry of a voltage-activated potassium channel. *Nature.* 350:232–235.

Magleby, K.L., and B.S. Pallotta. 1983. Burst kinetics of single calcium-activated potassium channels in cultured rat muscle. *J. Physiol. (Lond.).* 344:605–623.

Mannuzzu, L.M., M.M. Moronne, and E.Y. Isacoff. 1996. Direct physical measure of conformational rearrangement underlying potassium channel gating. *Science.* 271:213–216.

Marten, I., and T. Hoshi. 1997. Voltage-dependent gating characteristics of the K^+ channel KAT1 depend on the N and C termini. *Proc. Natl. Acad. Sci. USA.* 94:3448–3453.

Matsuda, H. 1991. Magnesium gating of the inwardly rectifying K^+ channel. *Annu. Rev. Physiol.* 53:289–298.

Miller, A.G., and R.W. Aldrich. 1996. Conversion of a delayed rectifier K^+ channel to a voltage-gated inward rectifier K^+ channel by three amino acid substitutions. *Neuron.* 16:853–858.

Nichols, C.G., K. Ho, and S. Hebert. 1994. Mg^{2+} dependent inward rectification of ROMK1 potassium channels expressed in *Xenopus* oocytes. *J. Physiol. (Lond.).* 476:399–409.

Papazian, D.M., X.M. Shao, S.-A. Seoh, A.F. Mock, Y. Huang, and D.H. Wainstock. 1995. Electrostatic interactions of S4 voltage sensor in *Shaker* K^+ channel. *Neuron.* 14:1293–1301.

Papazian, D.M., L.C. Timpe, Y.N. Jan, and L.Y. Jan. 1991. Alteration of voltage-dependence of *Shaker* potassium channel by mutations in the S4 sequence. *Nature.* 349:305–310.

Pongs, O., N. Kecskemethy, R. Muller, J.I. Krah, A. Baumann, H.H. Kiltz, I. Canal, S. Llamazares, and A. Ferrus. 1988. *Shaker* encodes a family of putative potassium channel proteins in the nervous system of *Drosophila. EMBO (Eur. Mol. Biol. Organ.) J.* 7:1087–1096.

Salkoff, L., K. Baker, A. Butler, M. Covarrubias, D. Pak, and A. Wei. 1992. An essential 'set' of K^+ channels conserved in flies, mice and humans. *Trends Neurosci.* 15:161–166.

Sanger, F., S. Nicklen, and A.R. Coulsen. 1977. DNA sequencing with chain-terminating inhibitors. *Proc. Natl. Acad. Sci. USA.* 74: 5463–5467.

Santoro, B., D.T. Liu, H. Yao, D. Bartsch, E.R. Kandel, S.A. Siegelbaum, and G.R. Tibbs. 1998. Identification of a gene encoding a hyperpolarization-activated pacemaker channel of brain. *Cell.* 93: 717–729.

Schachtman, D.P., J.I. Schroeder, W.J. Lucas, J.A. Anderson, and R.F. Gaber. 1992. Expression of an inward-rectifying potassium channel by the *Arabidopsis* KAT1 cDNA. *Science.* 258:1654–1658.

Schonherr, R., and S.H. Heinemann. 1996. Molecular determinants for activation and inactivation of HERG, a human inward rectifier potassium channel. *J. Physiol. (Lond.).* 493:635–642.

Schoppa, N.E., K. McCormack, M.A. Tanouye, and F.J. Sigworth. 1992. The size of gating charge in wild-type and mutant *Shaker* potassium channels. *Science.* 255:1712–1715.

Schoppa, N.E., and F.J. Sigworth. 1998*a*. Activation of *Shaker* potassium channels. I. Characterization of voltage-dependent transitions. *J. Gen. Physiol.* 111:271–294.

Schoppa, N.E., and F.J. Sigworth. 1998*b*. Activation of *Shaker* channels. II. Kinetics of the V2 mutant channel. *J. Gen. Physiol.* 111: 295–311.

Schoppa, N.E., and F.J. Sigworth. 1998*c*. Activation of *Shaker* potassium channels. III. An activation gating model for wild-type and V2 mutant channels. *J. Gen. Physiol.* 111:313–342.

Schroeder, J.I., and H.H. Fang. 1991. Inward-rectifying potassium channels in guard cells provide a mechanism for low-affinity potassium uptake. *Proc. Natl. Acad. Sci. USA.* 88:11583–11587.

Sentenac, H., N. Bonneaud, M. Minet, F. Lacroute, J.-M. Salmon, F. Gaymard, and C. Grignon. 1992. Cloning and expression in yeast of a plant potassium ion transport system. *Science.* 256:663–665.

Shao, X.M., and D.M. Papazian. 1993. S4 mutations alter the single-channel gating kinetics of *Shaker* K^+ channels. *Neuron.* 11:343–352.

Sigworth, F.J., and S.M. Sine. 1987. Data transformation for improved and fitting of single-channel dwell time histograms. *Biophys. J.* 52:1047–1054.

Smith, P.L., T. Baukrowitz, and G. Yellen. 1996. The inward rectification mechanism of the HERG cardiac potassium channel. *Nature.* 379:833–836.

Smith-Maxwell, C.J., J.L. Ledwell, and R.W. Aldrich. 1998*a*. Role of the S4 in cooperativity of voltage-dependent potassium channel activation. *J. Gen. Physiol.* 111:399–420.

Spector, P.S., M.E. Curran, A.R. Zou, M.T. Keating, and M.C. Sanguinetti. 1996. Fast inactivation causes rectification of the I_{Kr} channel. *J. Gen. Physiol.* 107:611–619.

Stevens, C.F. 1978. Interactions between intrinsic membrane proteins and electric field. An approach to studying nerve excitability. *Biophys. J.* 22:295–306.

Stühmer, W., F. Conti, H. Suzuki, X. Wang, M. Noda, N. Yahagi, H. Kubo, and S. Numa. 1989. Structural parts involved in activation and inactivation of the sodium channel. *Nature.* 339:597–603.

Sussman, M.R., N.D. DeWitt, and J.F. Harper. 1994. Calcium, protons and potassium as inorganic second messengers in the cytoplasm of plant cells. *In* Arabidopsis. Cold Spring Harbor Laboratory Press, Plainview, N.Y. 1085–1118.

Tempel, B.L., D.M. Papazian, T.L. Schwarz, Y.N. Jan, and L.Y. Jan. 1987. Sequence of a probable potassium channel component encoded at the *Shaker* locus of *Drosophila. Science.* 237:770–775.

Timpe, L.C., Y.N. Jan, and L.Y. Jan. 1988. Four cDNA clones from the *Shaker* locus of *Drosophila* induce kinetically distinct A-type potassium currents in *Xenopus* oocytes. *Neuron.* 1:659–667.

Trudeau, M.C., J.W. Warmke, B. Ganetzky, and G.A. Robertson. 1995. Herg, a human inward rectifier in the voltage-gated potassium channel family. *Science.* 269:92–95.

Tytgat, J., and P. Hess. 1992. Evidence for cooperative interactions in potassium channel gating. *Nature.* 359:420–423.

Véry, A.A., F. Gaymard, C. Bosseux, H. Sentenac, and J.B. Thibaud. 1995. Expression of a cloned plant K^+ channel in *Xenopus* oo-

cytes: analysis of macroscopic currents. *Plant J.* 7:321–332.

Yang, N., and R. Horn. 1995. Evidence for voltage-dependent S4 movement in sodium channels. *Neuron.* 15:213–218.

Zagotta, W.N., and R.W. Aldrich. 1990. Voltage-dependent gating of *Shaker* A-type potassium channels in *Drosophila* muscle. *J. Gen. Physiol.* 95:29–60.

Zagotta, W.N., T. Hoshi, and R.W. Aldrich. 1990. Restoration of inactivation in mutants of *Shaker* potassium channels by a peptide derived from ShB. *Science.* 250:568–571.

Zagotta, W.N., T. Hoshi, J. Dittman, and R.W. Aldrich. 1994*a*. *Shaker* potassium channel gating II: transitions in the activation pathway. *J. Gen. Physiol.* 103:279–319.

Zagotta, W.N., T. Hoshi, and R.W. Aldrich. 1994*b*. *Shaker* potassium channel gating III: evaluation of kinetic models for activation. *J. Gen. Physiol.* 103:321–362.

Zei, P.C. 1998. Voltage-dependent gating mechanisms of the KAT1 inwardly rectifying potassium channel. Ph.D. dissertation, Stanford University, Stanford, CA.